UILU-ENG 86-3610

Report No. 133

MECHANICS ASPECTS OF CRACK CLOSURE

by

Paul L. Lalor

Materials and Design Division
Department of Mechanical and Industrial Engineering

A Report of the

MATERIALS ENGINEERING - MECHANICAL BEHAVIOR

College of Engineering, University of Illinois at Urbana-Champaign

August 1986

ACKNOWLEDGMENT

This work was sponsored by the Fracture Control Program, College of Engineering, University of Illinois at Urbana-Champaign.

Sincere gratitude is expressed to my advisor, Professor Huseyin Sehitoglu, whose frequent discussions and work reviews throughout the entire phase of my Master of Science program proved invaluable.

The contributions of a fellow student, R. Craig McClung, are also greatly appreciated. I would also like to thank June Kempka, Celia Daniel, and Suzanne Palmer for their efforts in the preparation of the manuscript.

Finally, the support and encouragement provided to me by my family is the main reason I have been able to progress to this point in my life. Many thanks are expressed to them.

TABLE OF CONTENTS

LIST OF FIGURES

NOMENCLATURE

B	matrix relating incremental strains to incremental nodal displacements
c	notch radius
C	plastic modulus
$\Delta CTOD$	range in crack tip opening displacement
du	increment of displacement
$d\varepsilon_{ij}, d\varepsilon^e_{ij}, d\varepsilon^p_{ij}$	increment of total, elastic, and plastic strain
$d\bar{\varepsilon}^p$	equivalent plastic strain increment
$d\lambda$	scalar used in flow rule
$d\mu$	scalar used in hardening rule
$D_{ijk\ell}$	matrix of elastic constants
E	modulus of elasticity
f	von Mises yield function
$H_{ijk\ell}$	constitutive elasto-plastic matrix
ΔJ	range in J-integral
k	stiffness of truss element
K, K^{el}	stiffness matrix and elastic stiffness matrix
K, K_{max}, K_{min}	stress intensity factors
K_{open}	stress intensity at crack opening
ΔK, ΔK_{eff}	range in stress intensity and effective stress intensity
ℓ, ℓ_o, ℓ_s	cracklength, initial (sawcut) cracklength and stabilized cracklength
n_{ij}	normal to the yield surface
r	x-distance behind crack tip
$r_p, \Delta r_p$	maximum and reversed notch plastic zone size
R^p	load vector
R	stress ratio, minimum stress/maximum stress
S, S_{max}, S_{min}	applied stress level and maximum and minimum applied stress level
S_{clos}, S_{open}	applied stress level at crack closure and at crack opening
S_{ij}, s^c_{ij}	deviatoric stress and back stress tensor
$\Delta S, \Delta S_{eff}$	stress range and effective stress range
t	thickness and time
T	temperature
V	volume
$w, \Delta w$	maximum and reversed crack tip plastic zone sizes
x, y	coordinate axes at crack tip
X, Y	global coordinate axes located at notch center (FEM)
σ_{ij}	stress tensor

σ_o	yield stress in tension
α_{ij}	normal back stress tensor
δ	crack opening displacement
δ_{ij}	Kronecker Delta (identity tensor)
ψ	residual vector

1. INTRODUCTION

1.1 Background

The discovery by Elber [1-3] of the crack closure phenomenon has provided a rationale for, among other things, fatigue thresholds, stress ratio and overload effects on crack growth, and recently, 'small crack' behavior in fatigue. To date, much of the work in the field of crack closure has been experimental and has been limited to cases where linear elastic fracture mechanics representations were valid. Relatively few mechanics analyses of the crack opening and closure phenomenon have been performed in the elastic and inelastic cycling regime. The need exists for developing such analyses to provide insight into material factors and the nature of the applied loading that contribute to crack opening and closure behavior.

The dominant contribution to crack closure at intermediate and high crack growth rates is the result of residual plastic deformations and the ensuing compressive residual stresses in the wake of a growing fatigue crack. This mechanism, termed plasticity induced closure, results in a crack that remains closed for a significant portion of a fatigue cycle. Fatigue crack surface profiles and stress-strain fields can then be markedly different from those of a stationary (sawcut) crack. Since the crack growth rate is related to crack tip stress-strain fields and the ensuing crack tip displacements, it is necessary to establish how these parameters are altered in the case of a fatigue crack. The problem becomes most complicated for crack growth in inelastic strain fields and from notches where stresses and displacements on the crack line are influenced by the notch field.

In cyclic loading, the crack tip opens when all the compressive residual stresses in the wake of the crack have been overcome by the applied load. Therefore, an effective stress range, $\Delta S_{eff} = S_{max}-S_{open}$, is used as a basis for an effective stress intensity range, ΔK_{eff}, to accurately describe the crack tip stress-strain and displacement fields in fatigue. Elasto-plastic fracture mechanics parameters (ΔCTOD, ΔJ) modified for closure effects have been utilized when small scale yielding conditions were violated [4-7]. These parameters can also incorporate the effective stress range. The determination of ΔS_{eff} (or Sopen) has not been systematically considered for different crack lengths, stress states, material hardening cases, and geometries. Admittedly, this would involve a substantial computational and experimental effort.

Two other mechanisms causing crack closure, namely oxide induced closure and roughness induced closure have been proposed [8-12]. Oxide induced closure results from a build up of oxides and other corrosion debris on the surfaces of a crack and acts to decrease the effective stress range. The same results are realized in roughness induced closure but the cause here is irregularities and non-mating of the fracture surfaces. These two factors are most relevant near the threshold regime and are not considered in this study.

Crack opening and closure behavior and hence crack growth rates are influenced by state of stress [4,13-16]. Tests under s.s.y. conditions indicated that closure occurs along the entire crack front but to a much lesser extent in the mid-interior of the front than near the surface edge of the crack [14]. Near the surface, out of plane stresses are

zero (plane stress). Contrarily, in the interior, surrounding material restrains out of plane deformation resulting in zero total strain in that direction (plane strain). The triaxial stress state inhibits plastic yielding in plane strain and the residual crack tip displacements and closure levels are different from the plane stress case.

The yield strength and strain hardening behavior of the material influences crack opening and closure. However, these effects have not been systematically examined by others.

Crack length effect on closure has been studied with experiments and analytically (using Dugdale model) primarily for cases of plane stress. Experiments for cases approaching plane strain are difficult to perform and this aspect of the problem requires further study. For example, bulk measurement (back face strain gage, potential drop, elastic compliance, clip-on displacement gage at notch mouth) of closure reflects plane strain closure while surface measurements (strain gage close to crack tip, optical interferometry, photomicrographs of crack tip) provide closure levels for plane stress. In the case of physically small cracks and/or small crack tip displacements (opening, sliding) it is difficult to make accurate measurements using the above techniques. Also, closure levels may be a function of measurement location with respect to the crack tip [17].

1.2 Current Needs

The complexity of the crack closure problem necessitates reliable mechanics based approaches to characterize closure behavior. The

constitutive model (for the time-independent case) should have the capabilities to account for strain hardening (sometimes varying with cycles), the Bauschinger effect, and cyclic mean stress relaxation, observed in materials. General loading paths such as nonproportional loading should be handled. Large strain and geometry effects to account for blunting of the crack tip observed under plane strain/large strain conditions could also be incorporated into the formulation. Two extreme cases of the stress state (plane stress and plane strain) would provide guidelines on stress state influence on closure. Ideally, three-dimensional modeling of fatigue cracks should be considered but computational efforts needed to achieve this are enormous at the present time. The model should also allow cyclic crack growth based on a physical crack advance criteria. As yet, there has not been a universally accepted mechanism of fatigue crack advance, therefore, several criteria need be considered. The stress ratio, crack length, stress range (relative to the yield stress range), stress state (plane strain/stress and others) and influence of inelastic strain fields (gradients) must then be studied. The model should predict experimental crack opening and closure stresses with reasonable accuracy in these cases.

Successful, but limited, analytical models of fatigue crack closure based on the Dugdale strip-yield model [18] have been developed by a host of researchers [16,19-24]. The advantage of this approach is that extensive nonlinear analysis can be replaced with suitably superpositioned elastic solutions. These models require approximations or weight function methods to determine the plastic stretch deposited along

the crack surfaces since no closed form elasto-plastic solutions exist. The Dugdale model was developed for, and in most cases limited to, plane stress conditions in elastic-perfectly plastic materials subjected to small scale yielding. Dugdale solutions are available for only a limited number of geometries. These models have provided much insight into fatigue crack closure behavior. An extension of the original model is the incorporation of a 'constraint' factor on yielding to simulate, in an approximate way, plane strain conditions [16,23]. Strain hardening effects have also been attempted with modifications to the model [25,26], however, there are known limitations in this case [25] when results are compared to finite element work.

1.3 Current Work

A comparison of the capabilities of the analytical closure models with the previous description of the features thought required for a sound mechanics model reveals many limitations. Apart from element mesh sensitivity and crack advance criteria problems, elasto-plastic finite element (EPFE) techniques could theoretically satisfy all of the aforementioned model requirements and thus provide opening and closure levels of reasonable accuracy. Several studies [27-31] have applied EPFE to problems of fatigue crack closure. The present work involves the development and implementation of a fatigue crack closure model based on EPFE techniques. Although some of the aforementioned model capabilities are not presently included, the current work provides a good working model to aid in the better understanding of the closure phenomenon. The advantages and limitations of the EPFE approach to crack closure will be discussed.

The FE technique developed in this study is capable of simulating either plane stress or plane strain states in a strain hardening material. Provisions are made to change the boundary conditions associated with the intermittent contact and separation of the crack faces during cyclic loading. The crack tip is extended through the finite element mesh at prescribed points in the loading history. The specific variables known to effect crack closure and crack growth behavior that are concentrated on in this study include applied stress amplitude relative to yield stress, stress state, material hardening behavior (plastic modulus), crack length, and plastic wake with respect to total crack length. Two constant amplitude stress ratios, $R = 0$ and $R = -1$, are examined. Crack opening and closure stress levels, near crack stress fields, and crack opening displacements are determined for small and long crack cases. Comparisons of results are made with stationary cracks under monotonic loading conditions.

1.4 Purpose and Scope

The purpose of this study is to:

a) simulate the crack opening and closure behavior of the 1070 steel in a center notched geometry using elasto-plastic finite element methods and compare opening and closure results with experiments; discuss the influence of notch stress-strain and material hardening behavior on crack opening and closure.

b) determine the influence of physical crack length on plasticity induced crack opening and closure levels and the subsequent effect on fatigue crack growth rates

c) establish the variation of crack opening and closure behavior as the levels of constant amplitude loading are increased.

d) identify and quantify the variation of crack closure with state of stress for cracks growing from a circular hole.

e) discuss the benefits and drawbacks of studying the crack closure problem with elasto-plastic finite element methods.

2. ANALYSIS

2.1 Method Description

This section presents an outline of the specific problems that have been addressed and the method of analysis. Specifically, a fatigue crack growing out of a center notched plate (Fig. 1) subjected to constant amplitude mode I loading at stress ratios of R = -1 and R = 0 is analyzed. The crack is grown from initiation to a length comparable to the radius of the notch (c = 0.6 mm). Both the effects of state of stress at the crack tip and level of applied stress are systematically studied at different crack lengths. This particular geometry was chosen because the model to be presented here has been shown to provide an accurate simulation [30] of experimental crack closure studies performed on similar 1070 steel specimens [19,20]. The experimental stress-strain response and essential material properties are shown in Fig. 2. The C/E = 0.07 case corresponds to the 1070 steel material of interest where C is the plastic modulus. Analysis is also performed on a material with the same yield strength that strain hardens as C/E = 0.01. Comparisons are made to determine the influence of strain hardening on closure behavior.

A two dimensional elasto-plastic finite element model that accounts for cyclic crack extension and the changing boundary conditions associated with intermittent crack face contact is developed to study crack closure. The mesh in Fig. 3 consists of four noded isoparametric quadrilateral elements with a 2x2 integration rule. Attached to the nodes at the crack face are a series of variable stiffness truss elements. These elements are used to control constraints on dis-

placements associated with crack opening and closure as will be discussed later. Two mesh sizes (in the vicinity of the crack) were used in the study (Fig. 4) to determine the effect of discretization on predicted crack tip material behavior. Mesh A consists of 630 elements and 690 nodes while mesh B has 1140 elements and 1218 nodes. A typical element side length dimension in the vicinity of the crack is 0.028mm for mesh A and .014mm for mesh B. Nodal coordinates are updated after the application of each convergent load increment.

The schematics of Figs. 5 and 6 explain the crack opening and closure criteria. The location of the crack tip and notch surface are indicated in Fig. 5. The stress fields at maximum and minimum load are depicted in Fig. 6. In the finite element simulation, the coordinates of the nodes along the crack face are continuously monitored during incremental unloading to determine the point at which they return to their original $y = 0$ position (Fig. 5). At this point, opposing crack faces have made contact and constraint from further y-displacement is invoked. This is accomplished by making the value of the stiffness, k, of the truss element connected to this node equal to a very large number ($k \to \infty$). In this study, the applied stress level at which a node in the wake of the crack tip first returns to it's original $y = 0$ position during unloading is termed the crack closure level, S_{clos}. Note, on the average, each quarter cycle for $R = -1$ loading conditions (half cycle for $R = 0$) was divided into about twenty equal load increments.

With further unloading, residual compressive contact stresses are built up in the material elements comprising the wake of the crack tip

(Fig. 6). For R = -1 loading and the range of crack lengths considered, the entire crack is closed at minimum load. Note that for R = 0 loading, in many cases complete crack face closure had not occurred at minimum load consistent with analytical and experimental work [19,20]. Furthermore, in the R = 0 case, often first contact of crack surfaces occurred well behind the crack tip. The closure criteria used in this study to establish S_{clos} is that of first closure of crack surfaces and not complete crack face closure.

In order for the crack to reopen and propagate further, the residual compressive stresses must be overcome by the applied loading [2-3]. During the loading portion of a cycle, the compressive stresses in the crack face material points are continuously monitored (Fig. 6). When the sign of one of these material point stresses (σ_{yy}) changes from compressive to zero or slightly tensile, the stiffness of the associated truss element is changed to zero ($k \rightarrow 0$) thus permitting the crack faces here to open. Crack opening level, S_{open}, is defined as the applied load level at which all the compressive residual stresses in the wake of the crack tip have been overcome.

In some other models [27,28], crack opening criteria was based on a positive displacement of the boundary condition controlling spring. It is thought that this criteria may be influenced by the extremely large, but finite, stiffness value assigned to a closed spring. Opening behavior, then, may be influenced by this spring stiffness and not completely dictated by the behavior of the actual crack tip material.

Crack extension is achieved by releasing the present crack tip node ($k \rightarrow 0$) when the peak of each load cycle is reached. This is an arbi-

trary crack extension criteria that has been used in previous studies [27,31] of closure using EPFE. No detailed study has been made here on the possible effects on closure behavior that may result from a crack tip extension criteria that released nodes at other times in the loading history.

2.2 Finite Element Formulation

Inherently, nonlinear material response occurs at the crack tip in ductile materials. The basic variational principle used in linear finite element methods [32] is still applicable to nonlinear material problems. Here a set of 'linearized' equations are solved in an iterative fashion to arrive at a final successful solution. In this work the incremental iterative scheme implemented is the direct Newton-Raphson method [32] flow charted in Fig. 7. This flowchart is for load control conditions and the logic is somewhat different under displacement control. A schematic to accompany the flowchart is presented in Fig. 8. This scheme converges quadratically but requires continuous updating of the stiffness matrix, K. A small strain (deformation) formulation is employed in this work.

The equilibrium equations to be satisfied are independent of the chosen material law. The strain matrix, B, relates the change in strain to a given change in displacement, $d\varepsilon = B\, du$. Substituting this relation into the principle of virtual work gives the equation which must hold true to satisfy equilibrium conditions, $\psi = \int_V B^T \sigma \, dV - R = 0$. Here, R is the vector of nodal forces and the integral is evaluated element by element and assembled over the entire region in the usual

manner [32]. Any incorrect values of the stress distribution or displacement field will result in the 'residual vector', ψ, having a nonzero value. The terms ψ_0, ψ_1, and ψ_2 in Fig. 8 refer to the additional nodal forces required to bring the assumed displacement field into nodal equilibrium. The corresponding displacements are Δu_1, Δu_2, and Δu_3, respectively. Plasticity problems involving a nonlinear stress-strain relation require an iterative solution of 'linearized' equations to satisfy the relation, $\psi = 0$.

An appropriate constitutive relation and integration scheme are required to determine the increment of stress, $d\sigma$, associated with a given increment of strain, $d\varepsilon$. Subroutine UMAT, referred to in Fig. 7, is where this determination is made. The details of this analysis are given in the next sections.

2.3 Material Model

An incremental, rate independent, classical plasticity model is used in this study. Kinematic hardening is employed to best simulate the anisotropy (Bauschinger effect) associated with reversed yielding. With this rule, the yield surface maintains it's original dimensions but translates in stress space during plastic straining [33].

The initial yield condition according to von Mises is given by,

$$f(S_{ij},S^c_{ij}) = [\tfrac{3}{2}(S_{ij}- S^c_{ij})(S_{ij}- S^c_{ij})]^{\frac{1}{2}} = \sigma_o \qquad (1)$$

where σ_o is the initial yield stress in tension (a constant) and S_{ij} are the stress deviators given by,

$$S_{ij} = \sigma_{ij} - \tfrac{1}{3}\sigma_{kk}\delta_{ij} \qquad (2)$$

where σ_{ij} is the stress component vector and δ_{ij} is the Kronecker delta. S^c_{ij} represents the position of the center of the yield surface in deviatoric stress space due to work hardening. The center of the yield surface translates incrementally according to,

$$dS^c_{ij} = d\mu(S_{ij} - S^c_{ij}) \tag{3}$$

where $d\mu$ is a positive scalar to be determined.

The plastic strain increments are, based on Druckers postulate, in the direction of the outward normal to the yield surface. This flow rule is expressed as,

$$d\varepsilon^p_{ij} = d\lambda \frac{\partial f(S_{ij}, S^c_{ij})}{\partial S_{ij}} \tag{4}$$

where $d\lambda$ is a positive scalar during active plastic straining and zero for purely elastic responses. To evaluate $d\lambda$, the definition of the equivalent plastic strain increment $d\bar{\varepsilon}^p$ in [34] is used,

$$d\bar{\varepsilon}^p = \frac{1}{\sigma_o}(S_{ij} - S^c_{ij})\, d\varepsilon^p_{ij}. \tag{5}$$

Note that,

$$\frac{\partial f(S_{ij}, S^c_{ij})}{\partial S_{ij}} = \frac{3}{2\sigma_o}(S_{ij} - S^c_{ij}) \tag{6}$$

so (4) becomes,

$$d\varepsilon^p_{ij} = \frac{3d\lambda}{2\sigma_o}(S_{ij} - S^c_{ij}). \tag{7}$$

Substituting (7) into (5) gives,

$$d\bar{\varepsilon}^p = d\lambda \left(\frac{1}{\sigma_o}\right)^2 \frac{3}{2}(S_{ij} - S^c_{ij})(S_{ij} - S^c_{ij}) \tag{8}$$

which from (1) reduces to,

$$d\bar{\varepsilon}^p = d\lambda = \frac{1}{\sigma_o} (S_{ij} - S^c_{ij})\, d\varepsilon^p_{ij} \tag{9}$$

so (7) becomes,

$$d\varepsilon^p_{ij} = \frac{3}{2\sigma_o} d\bar{\varepsilon}^p (S_{ij} - S^c_{ij}) \tag{10a}$$

or,

$$d\varepsilon^p_{ij} = d\bar{\varepsilon}^p \frac{\partial f}{\partial S_{ij}}. \tag{10b}$$

During active plastic flow the consistency condition requires the stress state to remain on the translating yield surface. The yield condition, (1), must be continuously satisfied. Taking the total derivative,

$$\frac{\partial f}{\partial S_{ij}} dS_{ij} + \frac{\partial f}{\partial S^c_{ij}} dS^c_{ij} = 0. \tag{11}$$

It can be shown that the following relation in normal stress space is equivalent to (11) for an isotropic material,

$$\frac{\partial f}{\partial \sigma_{ij}} d\sigma_{ij} + \frac{\partial f}{\partial \alpha_{ij}} d\alpha_{ij} = 0 \tag{12}$$

where α_{ij} is the center of the yield surface in normal stress space,

$$S^c_{ij} = \alpha_{ij} - \frac{1}{3} \alpha_{kk} \delta_{ij}. \tag{13}$$

The strain rate, $d\varepsilon_{ij}$, can be broken up into elastic and plastic components,

$$d\varepsilon_{ij} = d\varepsilon^e_{ij} + d\varepsilon^p_{ij}. \tag{14}$$

In the elastic domain, stress increments, $d\sigma_{ij}$, can be related to elastic strain increments with the usual matrix of elastic constants, D, which depends on whether plane stress or plane strain conditions are being simulated [35].

$$d\sigma_{ij} = D_{ijk\ell}\, d\varepsilon^{e}_{k\ell} \tag{15}$$

or from (14),

$$d\sigma_{ij} = D_{ijk\ell}(d\varepsilon_{k\ell} - d\varepsilon^{p}_{k\ell}). \tag{16}$$

Ziegler's modification [33] of Prager's kinematic hardening rule indicates that the increment of translation of the center of the yield surface, dS^{c}_{ij}, is in the direction of the vector connecting the present center to the stress state as indicated by (3). The scalar $d\mu$ is related to the consistency condition, (12), and is taken as [34],

$$d\mu = C\,\frac{d\bar{\varepsilon}^{p}}{\sigma_o}. \tag{17}$$

Substituting (17) into (3),

$$dS^{c}_{ij} = C\,\frac{d\bar{\varepsilon}^{p}}{\sigma_o}\,(S_{ij} - S^{c}_{ij}) \tag{18}$$

here,

$$C = \frac{d\sigma}{d\bar{\varepsilon}^{p}} \tag{19}$$

is the slope of the stress versus plastic strain curve in uniaxial tension. Presently, a bilinear stress-strain curve is modeled so C = constant.

To obtain the relation between increments of stress and increments of strain we proceed as follows. Noting that,

$$\frac{\partial f}{\partial S_{ij}} = \frac{-\partial f}{\partial S^c_{ij}} = \frac{\partial f}{\partial \sigma_{ij}} \tag{20}$$

and,

$$\frac{\partial f}{\partial \sigma_{ij}} d\sigma_{ij} = \frac{-\partial f}{\partial S^c_{ij}} dS^c_{ij} \tag{21}$$

(16) becomes,

$$\frac{\partial f}{\partial \sigma_{ij}} d\sigma_{ij} = \frac{-\partial f}{\partial S^c_{ij}} dS^c_{ij} = \frac{\partial f}{\partial S_{ij}} D_{ijk\ell} d\epsilon_{k\ell} - \frac{\partial f}{\partial S_{ij}} D_{ijk\ell} \frac{\partial f}{\partial S_{k\ell}} d\bar{\epsilon}^p. \tag{22}$$

Substituting in (18) and rearranging,

$$\frac{\partial f}{\partial S_{ij}} D_{ijk\ell} \frac{\partial f}{\partial S_{k\ell}} d\bar{\epsilon}^p = \frac{\partial f}{\partial S_{ij}} D_{ijk\ell} d\epsilon_{k\ell} + \frac{\partial f}{\partial S^c_{ij}} \frac{C}{\sigma_o} d\bar{\epsilon}^p (S_{ij} - S^c_{ij}). \tag{23}$$

Considering (20) and the yield condition, (1), and solving (23) for $d\bar{\epsilon}^p$, we get,

$$d\bar{\epsilon}^p = \left[\frac{1}{\frac{\partial f}{\partial S_{ij}} D_{ijk\ell} \frac{\partial f}{\partial S_{k\ell}} + C}\right] \frac{\partial f}{\partial S_{ij}} D_{ijk\ell} d\epsilon_{k\ell}. \tag{24}$$

Now insert (10b) and (24) into (16) to get the relationship between stress increments and strain increments and the expression for the increment in back stress, dS^c_{ij}.

$$d\sigma_{ij} = \left[D_{ijk\ell} - \left(\frac{1}{\frac{\partial f}{\partial S_{rs}} D_{rstu} \frac{\partial f}{\partial S_{tu}} + C}\right)\left(D_{ijmn} \frac{\partial f}{\partial S_{mn}}\right)\left(D_{k\ell pq} \frac{\partial f}{\partial S_{pq}}\right)\right] d\epsilon_{k\ell} \tag{25}$$

$$dS_{ij}^{C} = \left[\frac{C}{\sigma_o} \frac{\frac{\partial f}{\partial S_{mn}} D_{mnrs}\, d\varepsilon_{rs}}{\frac{\partial f}{\partial S_{rs}} D_{rstu} \frac{\partial f}{\partial S_{tu}} + C}\right](S_{ij} - S_{ij}^{C}) \qquad (26)$$

Finally, update current stress, strain, and back stress values.

$$\sigma_{ij} = \sigma_{ij} + d\sigma_{ij}$$

$$\varepsilon_{ij} = \varepsilon_{ij} + d\varepsilon_{ij} \qquad (27a,b,c)$$

$$S_{ij}^{C} = S_{ij}^{C} + dS_{ij}^{C}$$

2.4 Numerical Integration of Rate Constitutive Equations

The constitutive equation of (25) can be expressed in the form,

$$d\sigma_{ij} = H_{ijk\ell}\, d\varepsilon_{k\ell}. \qquad (28)$$

The method implemented to integrate this equation over a finite time step is termed a "tangent stiffness, mean normal method with subincrementation and radial return." The method is described in part in the literature references [34,36-39]. The need for an elaborate integration scheme arises due to the sudden constraint encountered when the stress state reaches the yield surface in stress space. During active plastic straining, the stress state must remain on the translating yield surface.

A geometrical representation of the integration scheme in deviatoric stress space is depicted in Fig. 9. For generality, the initial (known) stress state, S_o, is in the elastic domain so that $f(S_o, S_o^C) - \sigma_o < 0$. The strain increment, $d\varepsilon_{k\ell}$, produced from a

prescribed load or displacement increment, Δu, causes a change in the present stress state, S_o.

The first step involved in determining the value of the new stress state is calculating a trial state, S_T, based on the assumption that the loading increment resulted in an entirely elastic response for the material point under consideration. S_T is calculated using Eq. (28) where for now $H_{ijk\ell}$ is simply the matrix of elastic constants relating stress to strain (Hookes Law). If $f(S_T, S_T^c) - \sigma_o < 0$, then the response truly was purely elastic and S_T is the correct new stress state. In this case, S_T will lie within the confines of the yield surface. If, however, $f(S_T, S_T^c) - \sigma_o > 0$, the loading has caused plastic straining and S_T is not the correct final stress state.

In the case of active plastic straining S_o is updated to the point where contact with the yield surface is first made. This state is termed S_c and satisfies the equation $f(S_c, S_c^c) = \sigma_o$. S_c is determined by assuming that strain varies linearly over the increment and calculating the fraction of the increment that is purely elastic. This fraction, q, is calculated from,

$$f(S_o + q\Delta S, S_o^c) - \sigma_o = 0. \qquad (29)$$

This requires solving a quadratic equation for q where the larger root in the range $0 \leq q \leq 1$ is taken as the correct value [34].

During the remainder of the strain increment, $(1 - q)d\varepsilon_{k\ell}$, there is active plastic straining and the elastic-plastic constitutive relation of Eq. (25) must be used for $H_{ijk\ell}$ in Eq. (28). For large strain increments, Schreyer, et al. [38] report a significant improvement in

accuracy if the remainder of the increment is broken up into subincrements. The number of subincrements, N, to be used in a given situation depends on the plastic strain rate direction since a primary source of error in this integration is the rotation of the normal to the yield surface during active plastic straining. Therefore, the normals to the yield surface, $n_{ij} = a \frac{\partial f}{\partial S_{ij}}$ (a = scalar), are calculated based on stress states S_T and S_C. If the angle between these two calculated normals is large many subincrements are used. As this angle approaches zero, the need for many subincrements is reduced so N is assigned a smaller value. The actual formula for N is based on numerical experience and in this work, equation 55 in reference [38] is used. The integration then proceeds subincrement by subincrement continuously updating both S_T and S_C.

In a given subincrement, the stress state S_M is calculated by,

$$S_M = \frac{1}{2} (S_T + S_C). \tag{30}$$

S_M is used to calculate the 'mean normal' to the yield surface, $n_{ij} = n_{ij}(S_M)$. This mean normal is used to calculate $H_{ijk\ell}$. $H_{ijk\ell}$ is then used in Eq. (28) to calculate the increment in stress which when added to S_C updates the stress state to S_A. In general, S_A will not lie on the yield surface but can be projected to it by a 'radial return'. This requires the determination of an adjusting factor, r, which is used to scale S_A down to S_F,

$$S_F = rS_A \tag{31}$$

where S_F satisfies the yield condition $f(S_F, S_F^c) - \sigma_o = 0$. r is determined iteratively. At this point the rest of the state variables are updated and the integration of this subincrement is complete.

3. RESULTS

This section describes the results of the crack growth simulation and crack closure determination. A center notched 2-D specimen (Fig. 3) in plane stress or plane strain is subjected to a series of different constant amplitude stress levels. Material stress state during the cyclic loading history of a typical material point ($x/c = 0.419$) along the crack line ($y = 0$) as the crack tip advances, approaches $x/c = 0.419$, reaches $x/c = 0.419$, and leaves $x/c = 0.419$ in the wake of the crack tip is depicted in Figs. 10 and 11. The stress states for $R = -1$ and $R = 0$ loading conditions are shown in Figs. 10 and 11, respectively. States of both plane stress and plane strain are given for comparative reasons in both figures. The components of stress at the point are given at both the maximum ($S = S_{max}$) and the minimum ($S = S_{min}$) levels of applied stress in a cycle. The symbol AY in the material element is present when the element is undergoing active plastic straining (Actively Yielding).

For a given stress ratio, due to the triaxial stress state developed under plane strain constraint, yielding is restrained. The crack tip plastic zone (and reversed crack tip plastic zone) is smaller in plane strain than the diffuse crack tip plastic zone that forms under plane stress conditions. One should note that due to the kinematic hardening model employed here the magnitudes of the stresses required to cause reversed plastic yielding during unloading are a function of the back stress components, α_{ij} (not shown in Figs. 10 and 11).

Reversed plastic deformation behavior of the material in the wake of the crack tip during unloading varies with R-ratio. Reversed yielding is present in the crack tip wake material at $S = S_{min}$ when $R = -1$ (Fig. 10) but not for $R = 0$ (Fig. 11). As an extreme example, the plane strain material point in the wake of the crack tip at $S = S_{min}$ (Fig. 11) has not even gone into compression for $R = 0$. In this instance it was found that this particular location ($x/c = 0.419$) of the crack flank had not made contact with the opposing crack face at $S = S_{min}$ hence no compressive stresses could be developed. This was more often the case for $R = 0$ loading than for the $R = -1$ case.

Numerically calculated crack surface profiles at $S = S_{max}$ for a crack that grew cyclically to a given length, ℓ/c, differ significantly from profiles of a crack that was initially sawcut to the same length. These profiles are shown for $\ell/c = 0.6$ in Fig. 12 for plane stress conditions and in Fig. 13 for plane strain conditions. The equations used to calculate stress intensity, K, in the normalization are given in Refs. [40,41]. The crack opening displacement of a growing fatigue crack is consistently lower than the ideal crack subjected to the same applied stress range. Note that the differences in the crack opening displacement, δ, in Figs. 12 and 13 are due not only to the lack of residual deformations on the ideal crack surface but are also contributed to by the existence of a greater effective stress intensity range, ΔK_{eff}, in the ideal crack case (ideal crack, $\Delta K_{eff} = K_{max} - K_{min}$, fatigue crack, $\Delta K_{eff} = K_{max} - K_{open}$).

Fatigue crack growth experiments by Sehitoglu [19,20] on center notched plates of 1070 steel were performed in an effort to characterize

crack opening and closure behavior under a set of controlled conditions. The validity of the current EPFE work was checked by attempting to simulate and thus predict some of the experimentally observed behavior seen in [20]. A comparison with experiment of the numerically predicted crack opening and closure levels as a function of growing crack length from the notch is provided in Fig. 14. The experimental technique in [19,20] consisted of a series of crack tip replicas taken at different crack lengths throughout the loading and unloading portions of constant amplitude cycles. These replicas were then viewed under a scanning electron microscope to determine the stress level at which the crack tip opened (S_{open}) and first closed (S_{clos}). Good agreement between the EPFE technique under plane stress conditions and experiment is observed over a wide range of crack length. Crack opening and closure levels were seen to increase then stabilize as the crack grew in length from the notch. Crack opening levels were consistently higher than closure levels.

A similar comparison with finite elements for conditions of R = 0 loading is presented in Fig. 15. Plane strain elements used in this simulation provide a better correlation with experiment than did plane stress elements. Once again, opening and closure levels vary with crack length measured from the notch but to a much lesser extent than for the R = -1 case. Here also, opening levels are somewhat higher than closure levels. This is a consistent trend throughout the work with the difference between opening and closure levels varying primarily with applied stress.

The global effects of both stress ratio, R, and applied stress level, S_{max}, on crack opening behavior are shown in Fig. 16 for plane stress conditions. R = -1 loading of a plane strain fatigue crack is included also. These curves were constructed by performing a series of numerical simulations each experiencing different applied stress levels. The opening stress level for a crack of length 0.48mm was plotted for each case. The trends clearly indicate that crack opening levels normalized by maximum applied stress decrease for cases run at higher applied stress levels. This trend is consistent with both analytical [16,24] and experimental [4] work of others. The rate of decrease of the ratio S_{open}/S_{max} with increasing S_{max}/σ_o is lower for R = 0 than for R = -1. At all load levels considered, the stress required to open the crack was higher for R = 0 than for R = -1.

In both Figs. 14 and 15 it is observed that after some amount of crack growth the crack reaches a length at which the opening stress levels begin to stabilize. This stabilized crack length, ℓ_s, is dependent on stress level, stress ratio, and state of stress, among other factors. From the construction of a series of curves in the form of Figs. 14 and 15, the approximate stable crack length values were extracted and plotted as a function of S_{max}/σ_o for both R = 0 and R = -1 loading conditions. Plane stress simulations and plane strain simulations are shown in Figs. 17 and 18, respectively. The cross hatched regions in these figures are the extent of maximum and reversed uncracked notch plastic zones, r_p and Δr_p, in the x-direction computed at the maximum and minimum stress levels, respectively. Note that the maximum notch plastic zone size, r_p, is independent of stress ratio,

and in the case of R = -1, is equal to the reversed plastic zone size, Δr_p. Under R = 0 conditions, however, Δr_p is, as indicated in the figures, a fraction of r_p. The influence of the notch plastic zone sizes on the 'small crack' growth problem is emphasized in section 4.

It is observed that stable crack length values are greater as higher applied stress levels act on the specimen and are clearly not confined to the reversed plastic zone of the notch. Crack lengths at stabilized opening levels are smaller for the R = 0 case than for the R = -1 case. This is partly a result of the variation of the notch stress fields at minimum load for the two stress ratio conditions as will be discussed later. More importantly, however, is the existence of reversed plastic deformation in the crack tip wake material at $S = S_{min}$ that occurs in most cases for R = -1 loading but to a lesser extent for R = 0 loading.

Differences in compressive residual stresses can be quantified by plotting the ratio of reversed crack tip plastic zone size, Δw, at $S = S_{min}$ to the maximum crack tip plastic zone size, w, at $S = S_{max}$ for the two stress ratios considered as a function of crack length. See Fig. 19. Observe that the ratio, $\Delta w/w$, is much lower at a given crack length and stress amplitude for R = 0 loading than for R = -1 loading. Since the absolute magnitude of w is not a strong function of stress ratio, this plot indicates the degree of reversed plasticity at the crack tip (and in the crack wake) to be much higher for R = -1 than for R = 0 in the cases shown.

Near crack stress fields will differ significantly depending on the material constraint conditions existing in a specimen. Plots of

normalized near crack stress fields, σ_{yy}/σ_o, at three different positions in the loading portion of a cycle, S/S_{max} = -1.0, 0.0, and 1.0, are shown in Fig. 20. The position on the x-axis at x/c = 0.0 represents the crack tip while the position at x/c = -ℓ/c indicates the notch surface. The stress field under plane stress conditions (Fig. 20), should be compared to Fig. 21 which illustrates the stress fields under plane strain conditions. Note that at low stress amplitudes plane strain opening levels are generally lower than plane stress levels, however, as will be shown later, this trend reverses at higher stress amplitudes. Among the notable differences between the two figures are the magnitudes of both the crack tip stress field at S/S_{max} = 1.0 and the crack wake residual stress field at S/S_{max} = -1.0. Specifically, the absolute values of these magnitudes are increased by the triaxial stress state existing under plane strain constraint. In turn, the presence of out of plane stresses, σ_{zz}, restricts the crack tip plastic zones to a smaller region in plane strain than in plane stress where σ_{zz} = 0.

The predicted crack opening stresses normalized by maximum stress, S_{open}/S_{max}, as a function of applied stress for both plane stress and plane strain conditions for a series of progressively increasing normalized crack lengths, ℓ/c, are summarized in Figs. 22, 23, and 24. As the crack lengths increase, the values of S_{open}/S_{max} increase indicating the effect of progressively longer wake regions containing plastically deformed material. Clearly, this analysis supports that the extent of plasticity induced closure increases with crack length. This crack length effect is most pronounced for R = -1 conditions. The

influence of stress state on opening levels is negligible at the smallest crack length shown, $\ell/c = 0.14$, where there is little wake length to create a strong closure effect. However, as the fatigue crack grows, stress state effects become more predominant.

Crack surface displacements are consistent with opening stress levels for the two states of stress considered. The surface profiles of a small crack ($\ell/c = 0.14$) at maximum load for both plane stress and plane strain conditions are shown in Fig. 25. The profiles are plotted for a high and a low applied stress level. It can be seen from Fig. 22 that the opening levels (hence effective stress ranges) for this particular crack length are equal for both stress states considered. Plane stress displacements are greater than those seen in plane strain. This behavior is also evident with ideal cracks upon comparison of Figs. 12 and 13.

For longer cracks subjected to $S_{max}/\sigma_o = 0.8$, the analysis predicts opening levels in plane stress lower than those for plane strain (Fig. 24). In this case, plane stress displacements exceeded plane strain displacements for a growing fatigue crack (Fig. 26) as well as for an ideal crack. However, when $S_{max}/\sigma_o = 0.4$ plane strain opening levels are considerably lower than plane stress levels. The resulting crack tip displacements in plane strain exceed those in plane stress consistent with the different effective stress range for both cases (Fig. 26).

In many fatigue analyses that consider closure effects, a common assumption is that opening and closure levels are approximately equal. In Fig. 27, which is a continuation (in crack length) of the series of

plots in Figs. 22-24 but with closure levels included also, it is seen that this assumption is generally valid at low stress amplitudes but breaks down at higher stresses. The difference between crack opening and closure stresses increases as the applied stress levels become greater. This phenomenon has been seen experimentally in another steel [42] and has implications in crack retardation and acceleration effects occurring after an overload [4].

In Fig. 28, crack opening levels are plotted as a function of applied stress level for the plane stress case when the loading conditions are R = 0. The curves were constructed for four different crack lengths. Increasing crack length results in higher opening levels, but again, it is clear that the crack length effect on closure is not as predominant as in the R = -1 loading case. Also, the influence of a greater applied stress level for a given crack length is relatively weak in the R = 0 case compared to the R = -1 case for the range of applied stress levels considered.

The fraction of crack length over which residual displacements (and stresses) exist influences crack closure behavior. Figure 29 is a plot of normalized crack opening level as a function of crack length measured from the notch. The analysis producing the solid curve was performed, as previously described, with an initial crack length of zero. The crack initiated directly out of the notch. The dashed curve, however, was generated from an analysis that started with an initially sawcut crack (measured from the notch) of length, $\ell_o/c = 0.234$. The lack of equivalent deformation and residual stress field histories behind the current crack tip in the two cases results in different crack opening

levels. Complete modeling of prior history, therefore, is an essential feature in predicting crack opening and closure behavior with the finite element method.

The outlined method could be used to describe closure behavior in a wide array of materials obeying an elasto-plastic constitutive law. The influence of the input material constants on closure behavior should be addressed. Much of the previous work of others [16,23,24,27] has modeled aluminium-like materials which exhibit little or no strain hardening (perfect plasticity). A plot of opening levels for a crack of length $\ell/c = 0.327$ as a function of applied stress for two materials with different strain hardening behavior is shown in Fig. 30. The 1070 steel has been modeled with a plastic modulus to elastic modulus ratio of $C/E = 0.07$ (Fig. 2). A ratio of $C/E = 0.01$ is used to determine the closure behavior of a fatigue crack in a material that hardens to a much lesser extent than the 1070 steel but with the same yield stress. Under the depicted conditions ($R = -1$, plane stress) the fatigue cracks in the material with the lower strain hardening characteristics ($C/E = 0.01$) open at lower stress levels than a comparable situation in a material that exhibits a greater degree of strain hardening.

The crack surface profiles for the two materials at the peak of the cycle for $S_{max}/\sigma_o = 0.4$ reveal the greater deformation existing in the lower strain hardening material. See Fig. 31. When the same analysis was performed under plane strain conditions the influence of strain hardening on both opening levels and deformation was far less than the plane stress case revealed. This is shown in Figs. 32 and 33.

4. DISCUSSION

The results of the analysis consistently depicted a crack length effect on closure behavior. Namely, crack opening and closure levels were observed to increase then stabilize as the crack grew away from the notch surface. Experimental observations (Figs. 14, 15) confirm this behavior (also, Ref. [19,20,43]). A previous work [30] showed that effective stress intensity ranges, calculated using the numerically predicted opening levels, correlated experimentally observed crack growth rates quite adequately even in the physically small crack length range. The variation of opening level is related to the size of the wake region of plastically deformed material.

There have been some accounts of small crack growth rate data merging with long crack data at crack lengths approximately coinciding with the original notch plastic zone size [44,45]. The present analysis predicts that crack opening levels are still quite transient at crack lengths considerably greater than either the reversed or maximum notch plastic zone size at all load levels studied (Fig. 18). In Fig. 17, at higher stress amplitudes, note that opening levels had stabilized at crack lengths within the maximum notch plastic zone size for R = 0 loading under plane stress conditions. The observed behavior of the growth rates of small fatigue cracks and the size of the original notch plastic zone cannot then be directly related if plasticity induced crack closure is thought to be the sole controlling phenomenon behind the 'small crack effect'. Other factors contribute to the end result.

Incorporation of crack opening levels into the calculation of crack growth rate correlating parameters has accounted for the effects of the

stress ratio, R, in experimental observations [43]. Certainly, the data shown in Fig. 16 reveals substantial differences in opening levels (plane stress) for a particular stress amplitude as a function of stress ratio which, evidently, accounts for the differences in observed crack growth rates. The level of the compressive stresses developed in the wake and at the tip of the crack at $S = S_{min}$ for the two R-ratios accounts for the differences in the subsequent opening levels attained [27].

The notch is as much a stress riser in compression as it is in tension for R = -1 loading after full crack face contact has been made. During unloading the presence of the notch tends to increase the ratio $\Delta w/w$ for shorter crack lengths embedded in the notch plastic zone (Fig. 19). This is not the case for R = 0 loading for the range of stress levels considered because in many cases full crack face contact has not been attained at $S = S_{min}$. Therefore, in the R = 0 cases, the influence of the notch on crack closure is confined to smaller crack sizes.

The dependence of $\Delta w/w$ on stress level is depicted in Fig. 19. The higher $\Delta w/w$ ratios result in lower values of S_{open}/S_{max} (see Figs. 16,22-24,27-28,30 and 32.) predominantly for R = -1 loading. The rate of decline of S_{open}/S_{max} with increasing stress levels is far greater for R = -1 loading than it is for R = 0.

Closure levels become lower than opening levels rapidly at higher stresses for a given R-ratio (especially R = -1). Implications of this phenomenon were pointed out by McClung and Sehitoglu [4]. Application of an overload in the high strain regime provides an acceleration effect.

Opening and closure behavior has been shown to change with the two stress states (plane stress and plane strain) considered in this study. At lower stresses ($S_{max}/\sigma_o < 0.6$), a general statement can be made that plane stress opening levels are greater than plane strain levels. The analysis showed this trend to reverse at high stresses but it would be rather unrealistic to expect the constraints associated with plane strain conditions to prevail at such high stress levels. EPFE techniques are a valuable tool in the study of constraint effects on crack closure since experimental observations of these effects are quite difficult to perform [13-15]. McClung And Sehitoglu [4] present crack growth rate correlations where state of stress was incorporated into the crack growth relation.

Relatively few research efforts have been directed at determining the effects of material parameters on closure behavior. The influence of basic material parameters such as elastic modulus, yield strength, and strain hardening rate have not been fully studied. The simulations of fatigue crack closure performed in this study provided a qualitative look at the effects of varying the degree of strain hardening on crack opening levels (Figs. 30-33).

Under plane stress conditions, where plastic flow is not constrained, there exists a large degree of difference in the amount of deformation existing between the materials exhibiting the two different strain hardening characteristics. The material with lower strain hardening (C/E = 0.01) experienced a higher crack tip plastic strain range at a given stress level than the higher strain hardening material (C/E = 0.07). Lower crack opening stresses for C/E = 0.01 than for C/E = 0.07 resulted.

In contrast, the same comparison under conditions of plane strain resulted in little or no difference in crack opening stresses (Fig. 32). Apparently, the strong constraint on yielding in plane strain resulted in deformations where the sensitivity to elastic-plastic behavior was less pronounced than for plane stress.

A few comments on the drawbacks of EPFE techniques in the study of fatigue crack closure here would be instructive. The single most important consideration being a high degree of near crack mesh refinement to insure as accurate results as possible. Newman [27] indicates that crack opening and closure levels can differ quite significantly from one mesh to another depending on the ratio of incremental crack extension (crack tip element side length) to current crack tip plastic zone size, w. This ratio should be kept as small as possible to insure accuracy. This is a difficult objective to achieve especially at low stress amplitudes under plane strain conditions and at high R-ratios where reversed crack tip plastic zone sizes are extremely small. In the present work an attempt was made to use higher order elements (4-noded isoparametric rather than constant strain triangular) to reduce the significance of mesh refinement. However, as yet no comparisons of results have been made with similar case studies incorporating triangular elements. A problem inherent with the use of isoparametric elements at a crack tip is that they must be refined enough so that the yield limit is exceeded at least at the inner integration point(s).

Throughout this work both mesh A (Fig. 4) and mesh B were used to insure that reported opening levels were not being falsely influenced by

lack of proper mesh refinement. Differences in opening levels between the two meshes were negligible at high stress levels ($S_{max}/\sigma_o > 0.6$) and below this stress level, mesh B results were more dependable. The largest discrepancies resulted for the plane strain, low stress level, R = 0 case studies. Under these circumstances, opening levels for mesh A were lower than mesh B by more than 10 percent and neither mesh was thought to provide adequate results. Further sensitivity studies on this issue are required.

Other drawbacks of the method are the lack of a good physical crack extension criteria (and knowledge of its subsequent effect on predicted closure behavior) and the large amount of computational time and memory required to perform the analyses.

5. CONCLUSIONS

1.) Experimental crack opening and closure levels of cracks growing from a notch were predicted accurately with the EPFE technique developed.

2.) The ratio S_{open}/S_{max} decreased with increasing applied stress levels for both plane stress and plane strain states. This ratio decreased more rapidly for a state of plane stress than for plane strain, and more rapidly under R = -1 loading than R = 0 loading.

3.) The difference between crack opening and crack closure levels becomes more significant at high applied stress levels.

4.) Stress state has an important influence on crack closure behavior and crack tip stress strain fields and EPFE techniques seem to quantify these effects.

5.) Closure behavior as influenced by stress ratio is linked to reversed yielding during unloading in the material in the vicinity of the crack tip.

6.) Crack opening levels increase to a stabilized value as the crack length increases. This is especially evident in crack growth from notches under completely reversed, R = -1, loading.

7.) Transient changes in opening and closure levels occur at crack lengths well past both the maximum and the reversed plastic zone size of the notch.

8.) Crack tip displacements for a fatigue crack were consistently lower than for an ideal crack subjected to the same applied stress range.

9.) Lower strain hardening characteristics in a material tend to decrease the fatigue crack opening stress levels in plane stress. In

plane strain the influence of strain hardening appears small for the cases considered.

10.) The crack opening and closure levels were lowered when the plastic wake of the crack growing from the notch was removed. The asymptotic opening level for a crack with limited wake is lower than the same crack length with full wake.

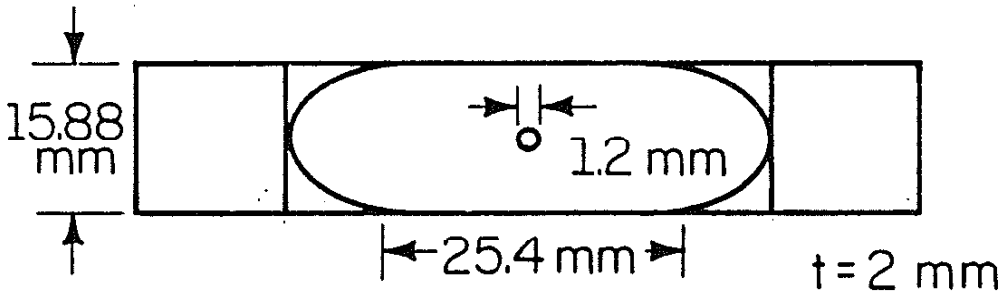

Figure 1 Center Notched Plate Geometry

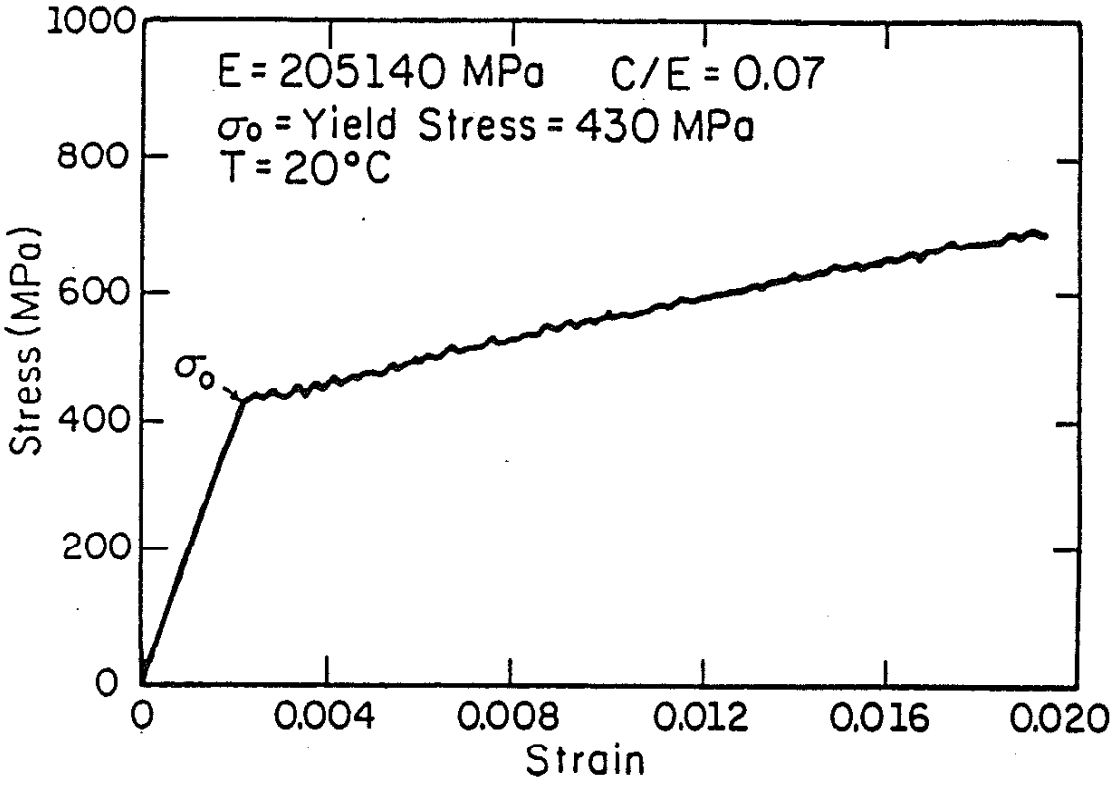

Figure 2 Experimental Stress-Strain Response for 1070 Wheel Steel (Class U)

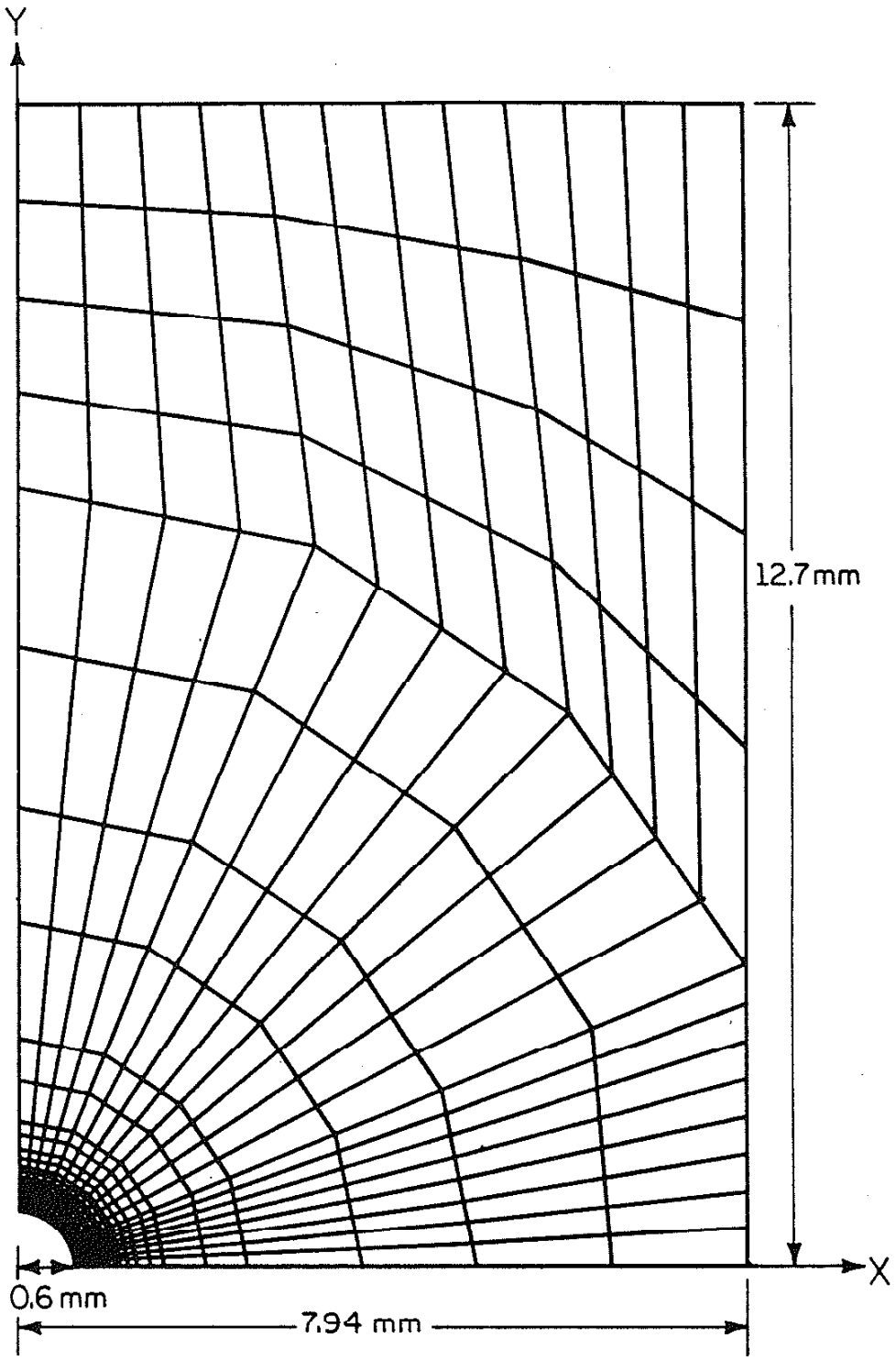

Figure 3 Finite Element Mesh for Center Notched Member

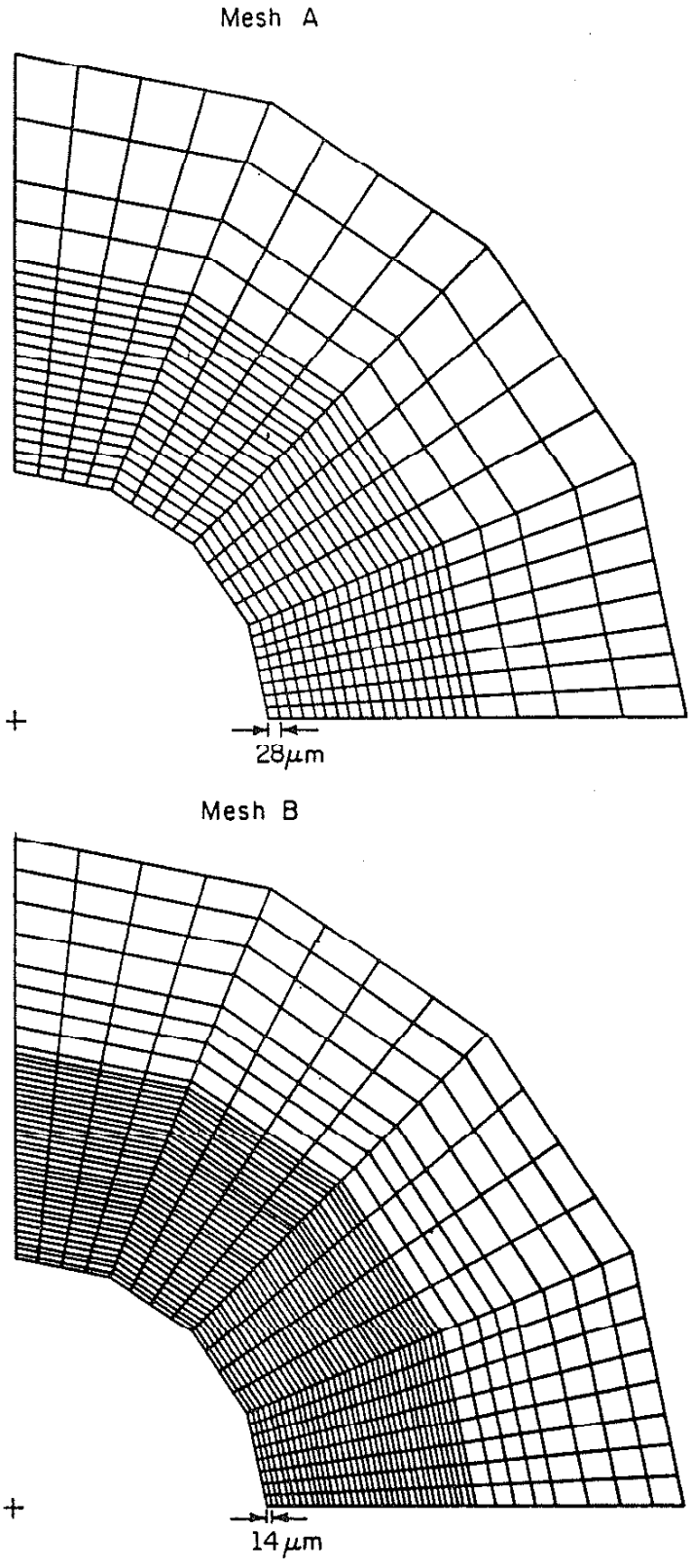

Figure 4 Near Crack Mesh Refinement for Meshes A and B

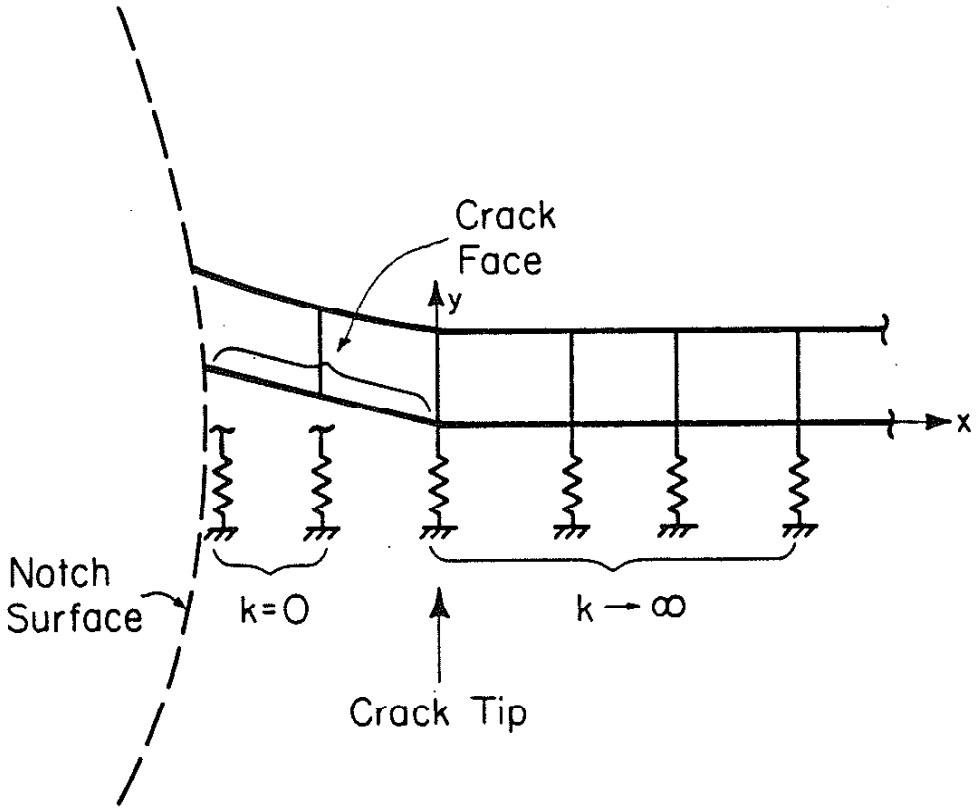

Figure 5 Representation of Boundary Condition Control along Crack Face

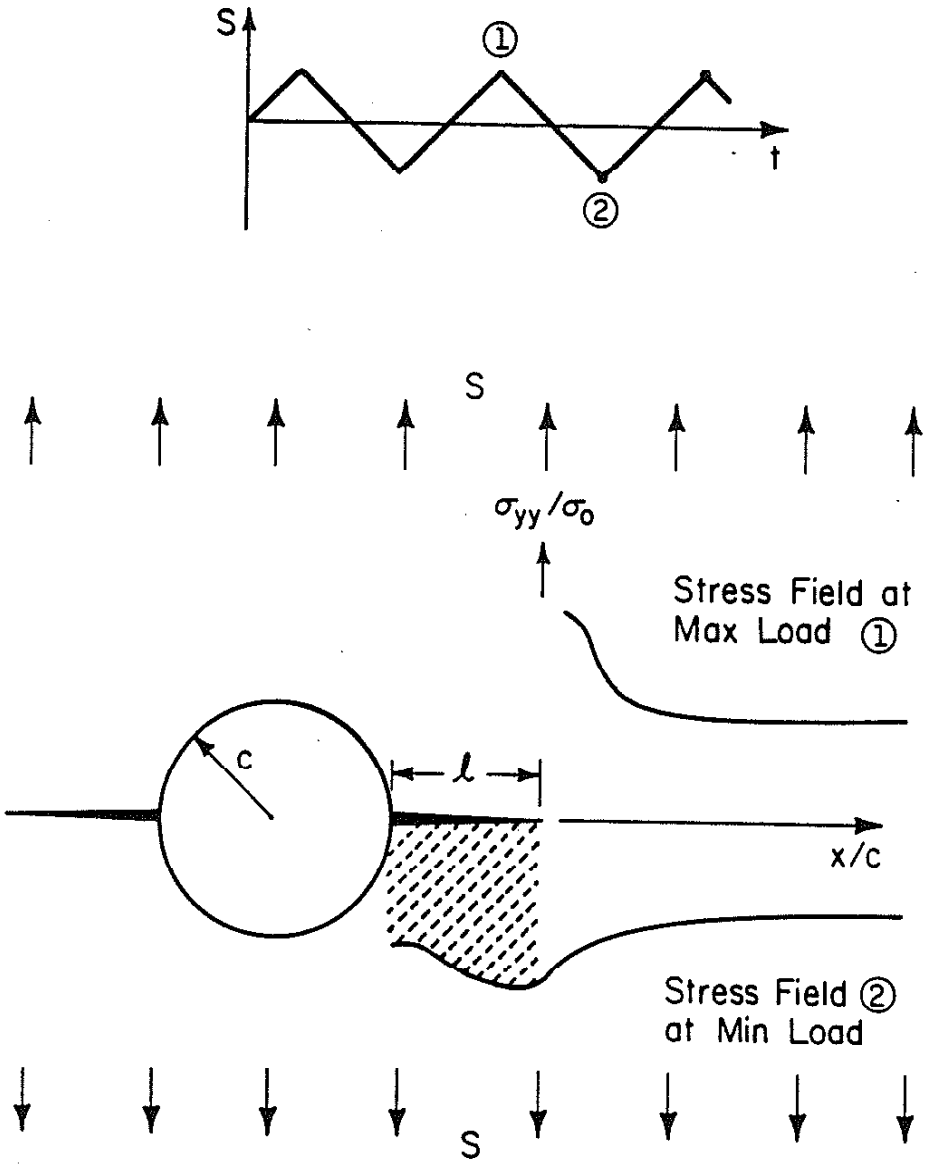

Figure 6 Schematic of Crack Opening and Closure Criteria

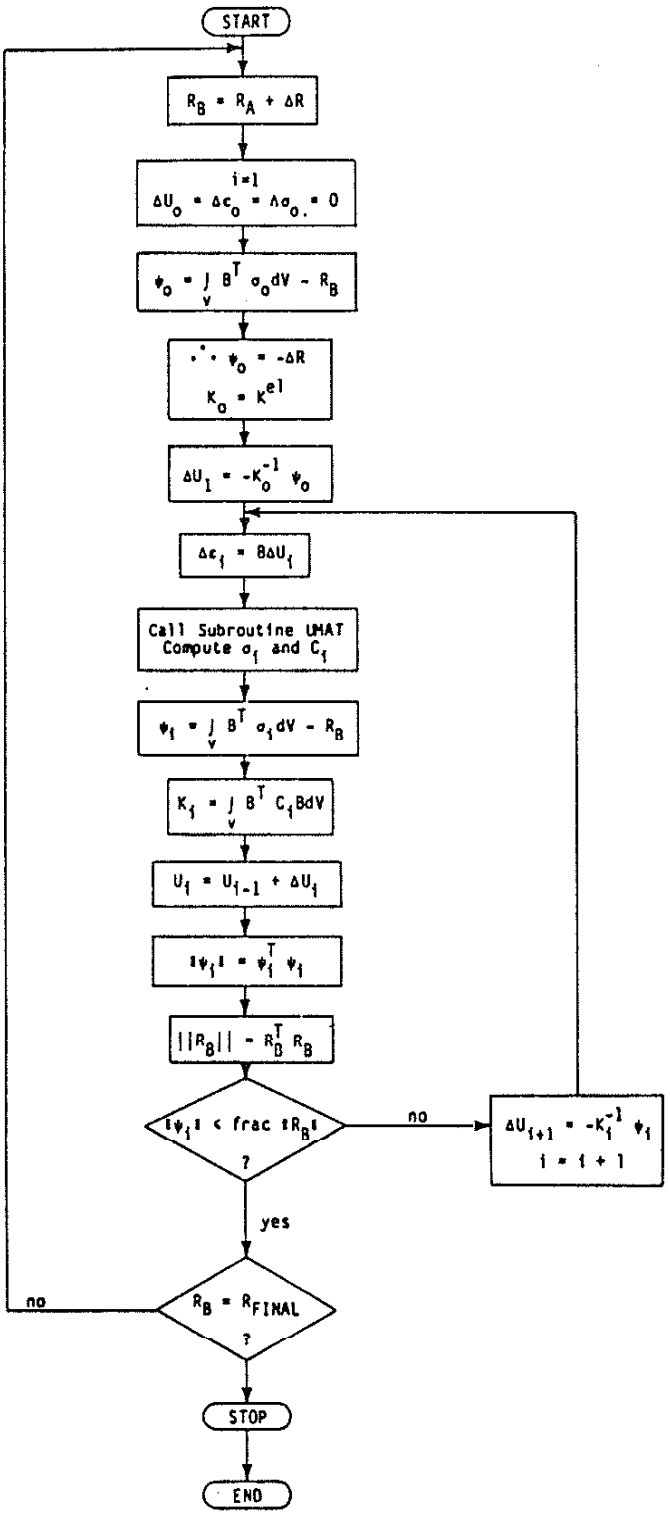

Figure 7 Flowchart for Newton-Raphson Iteration Scheme

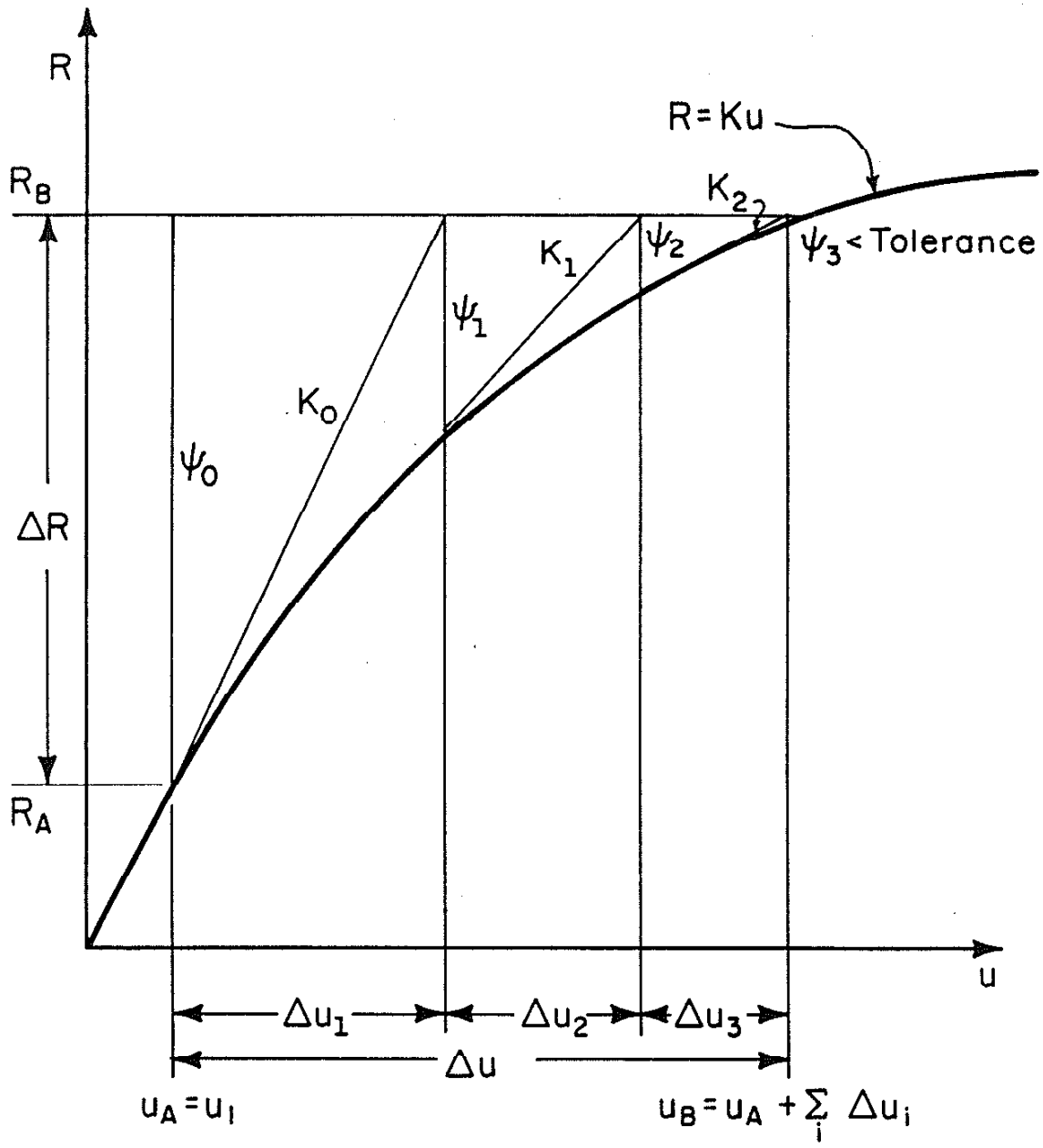

Figure 8 Schematic of Newton-Raphson Method

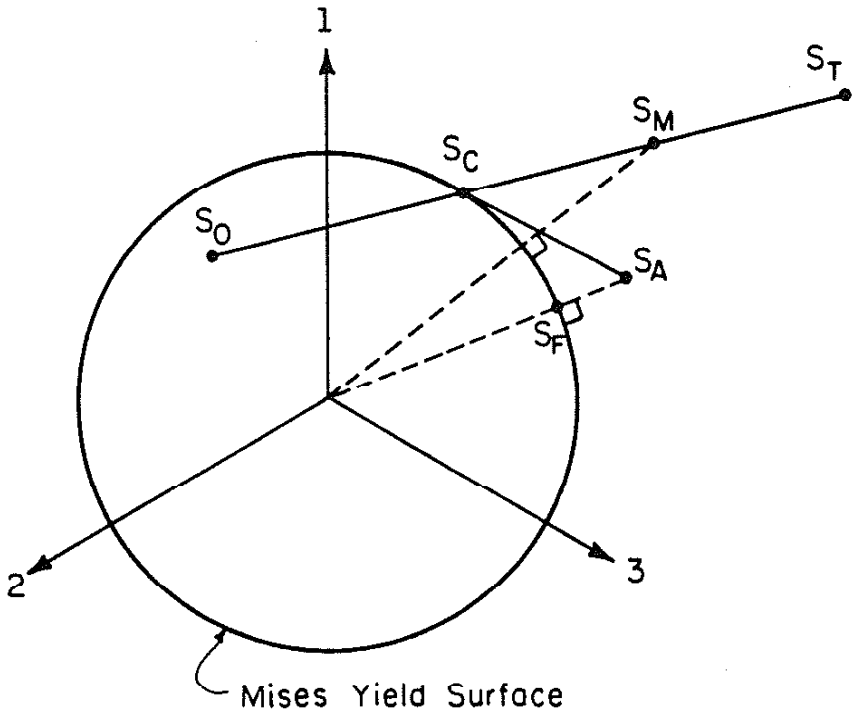

Figure 9 Geometrical Interpretation of the Method of Integration of the Rate Constitutive Equations

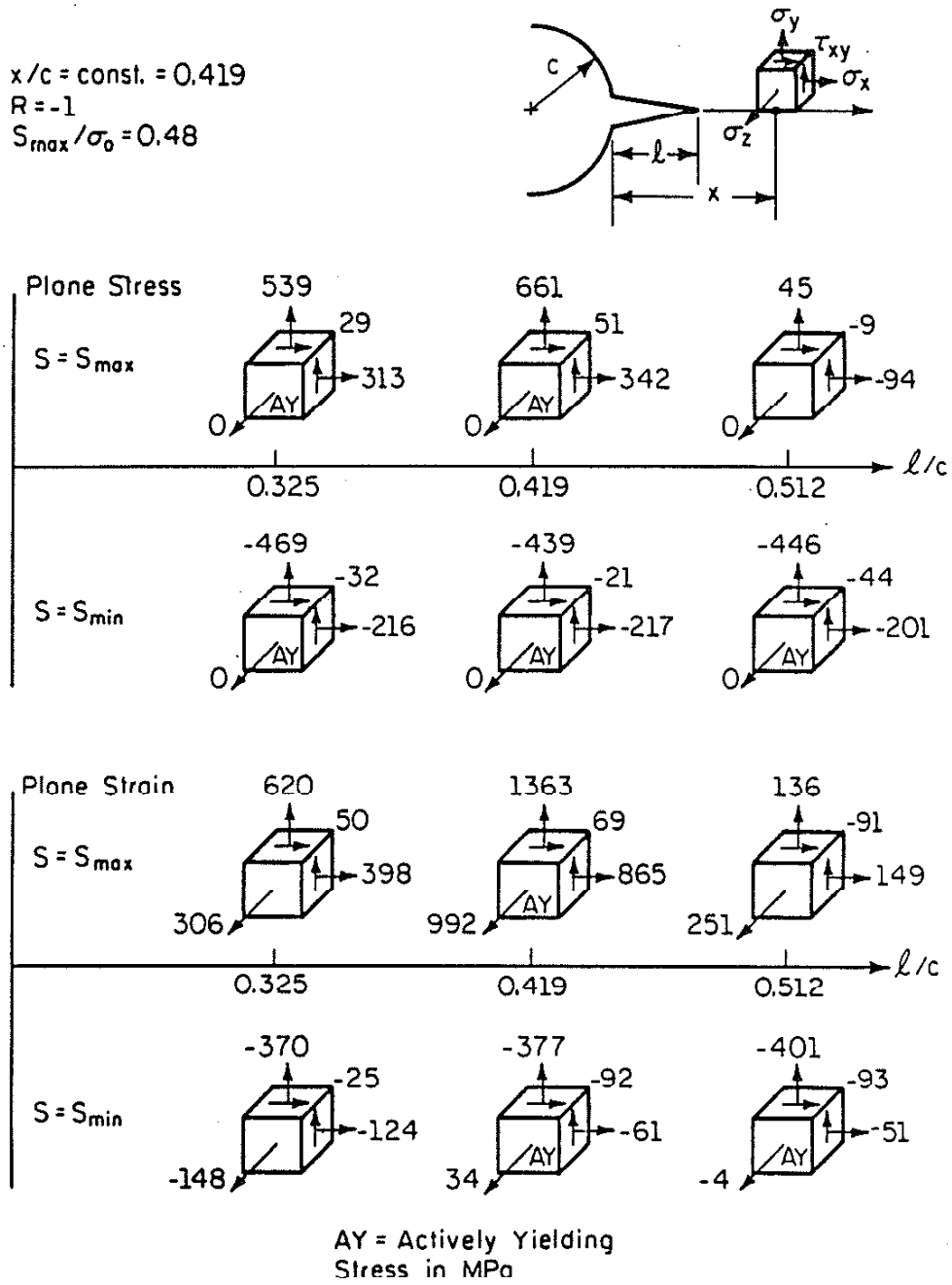

Figure 10 Crack Line Material Element Response as Fatigue Crack Passes through it (R = -1)

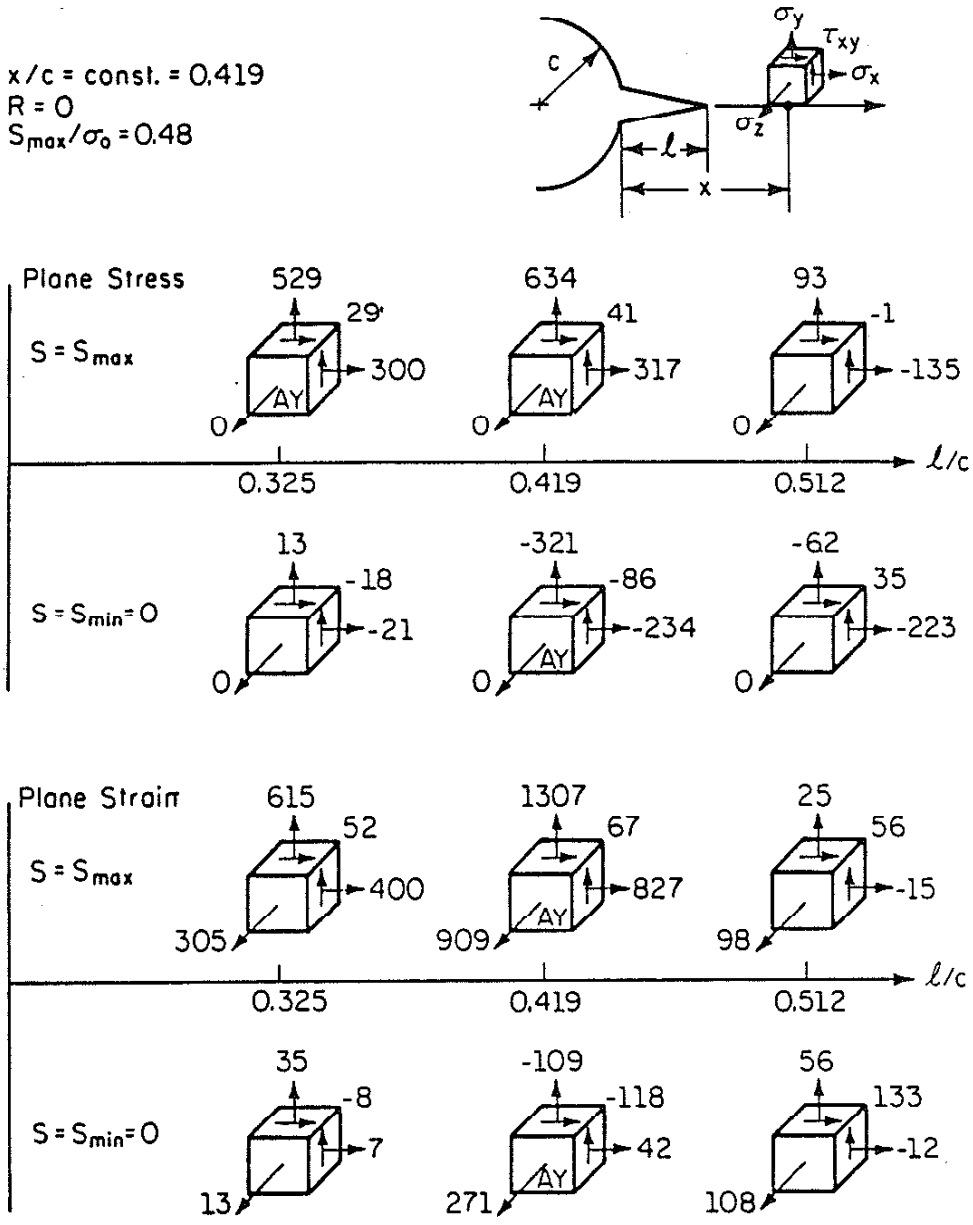

Figure 11 Crack Line Material Element Response as Fatigue Crack Passes through it (R = 0)

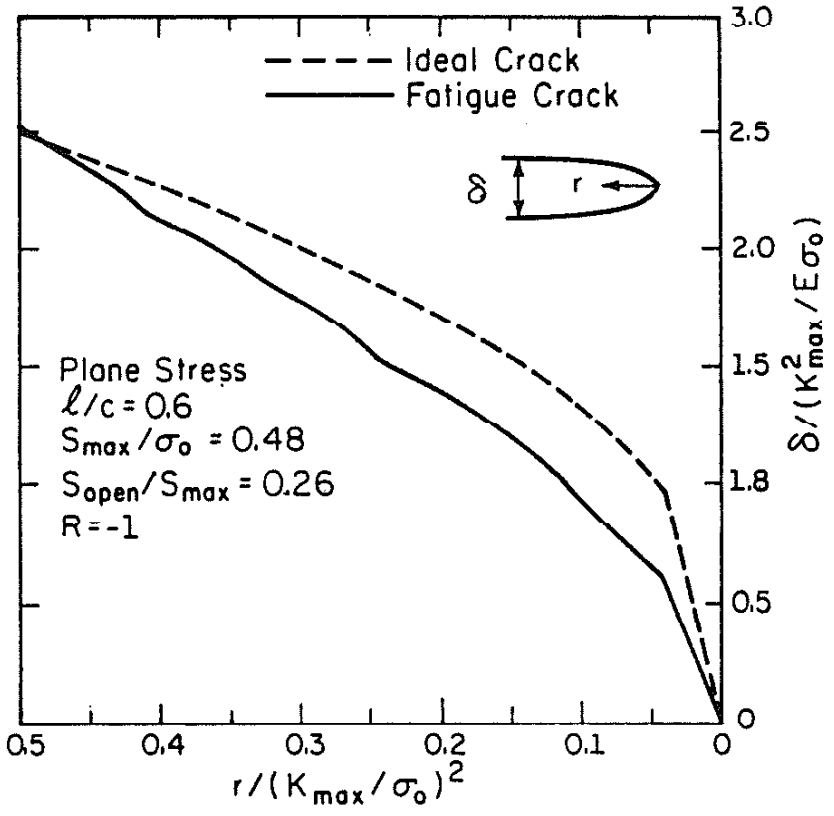

Figure 12 Plane Stress Crack Surface Profiles
Ideal Crack versus Fatigue Crack

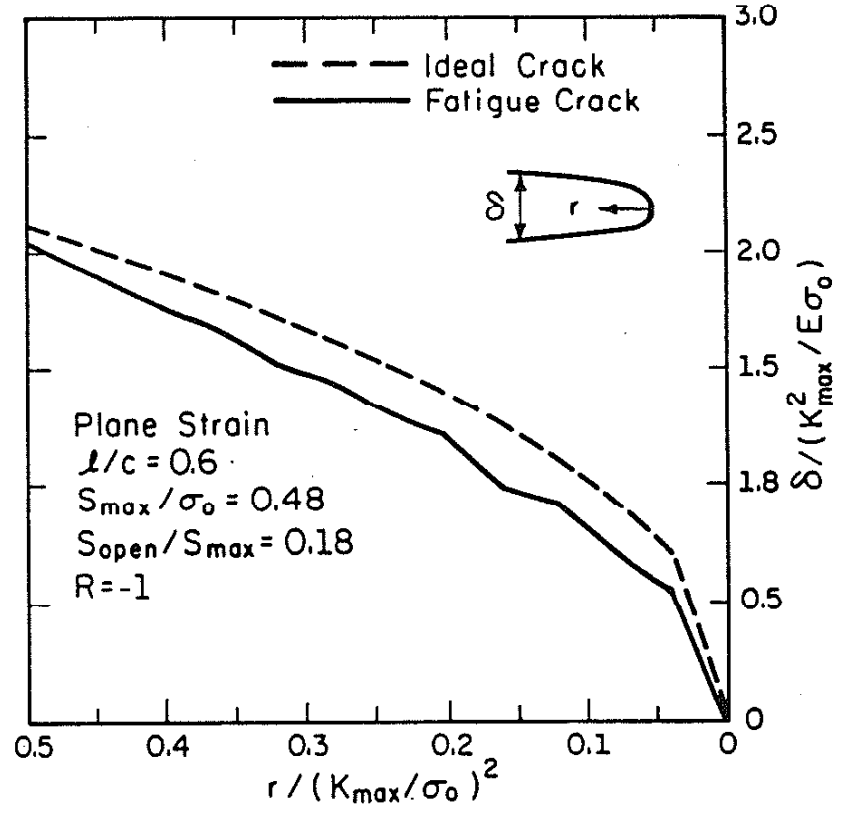

Figure 13 Plane Strain Crack Surface Profiles
Ideal Crack versus Fatigue Crack

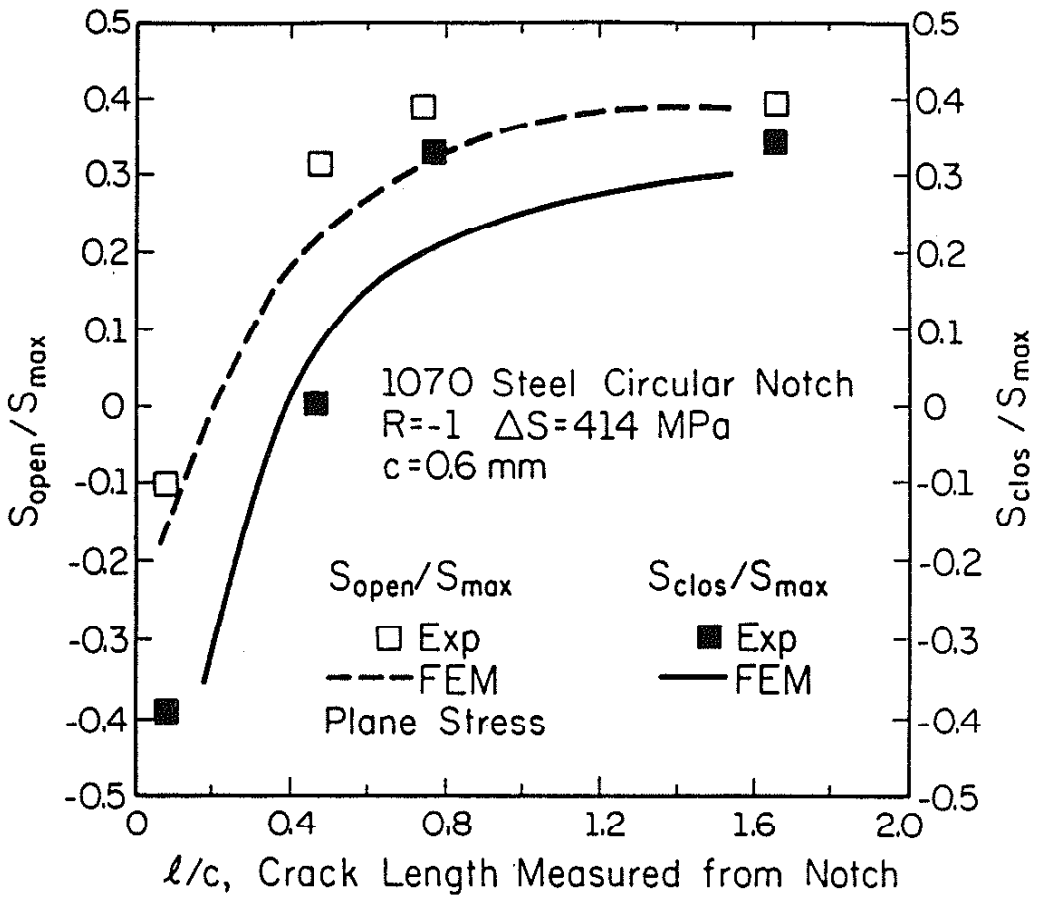

Figure 14 Experimental and Numerical Crack Opening and Closure Levels as Crack Grows from Notch (R = -1)

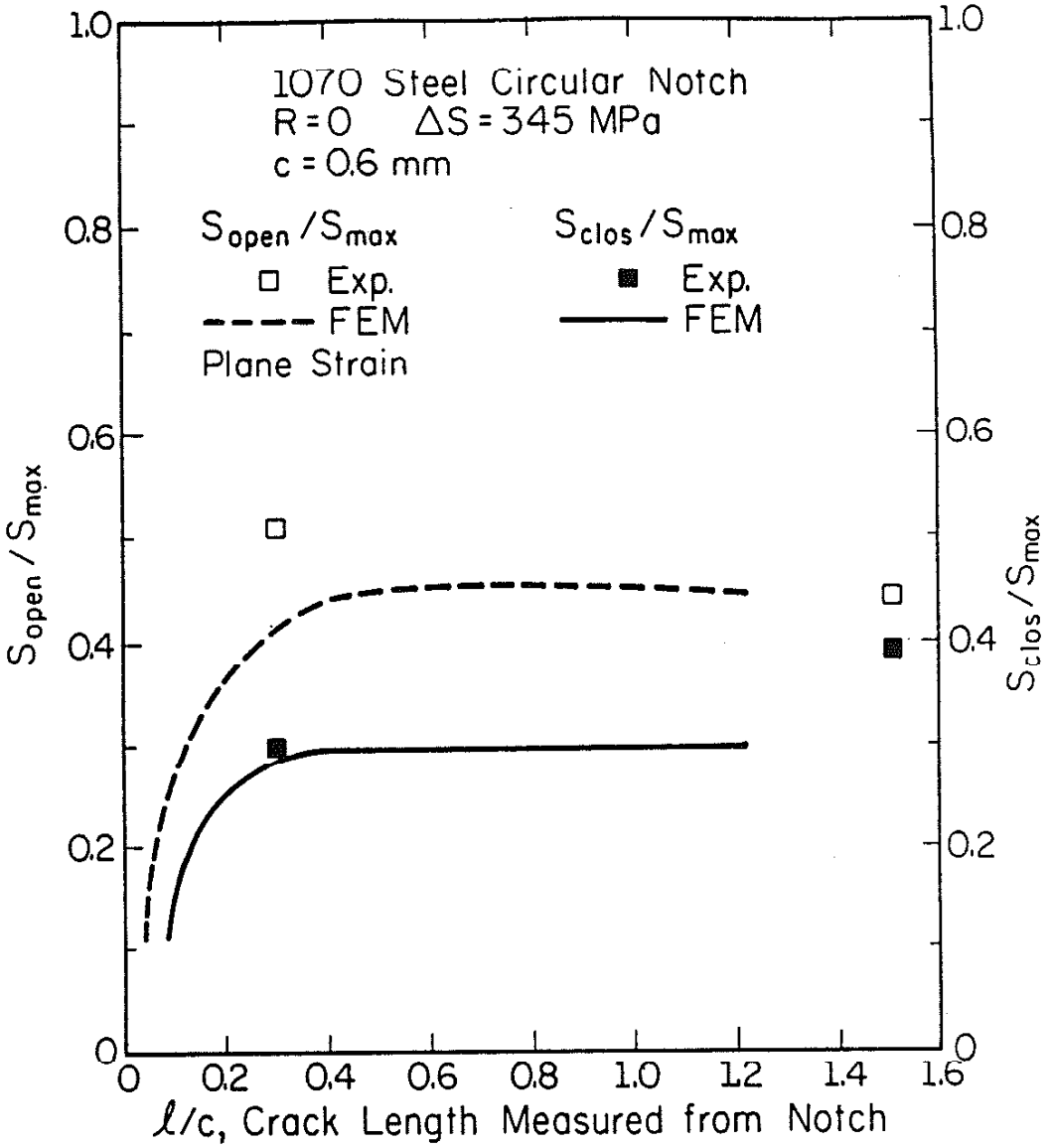

Figure 15 Experimental and Numerical Crack Opening and Closure Levels as Crack Grows from Notch (R = 0)

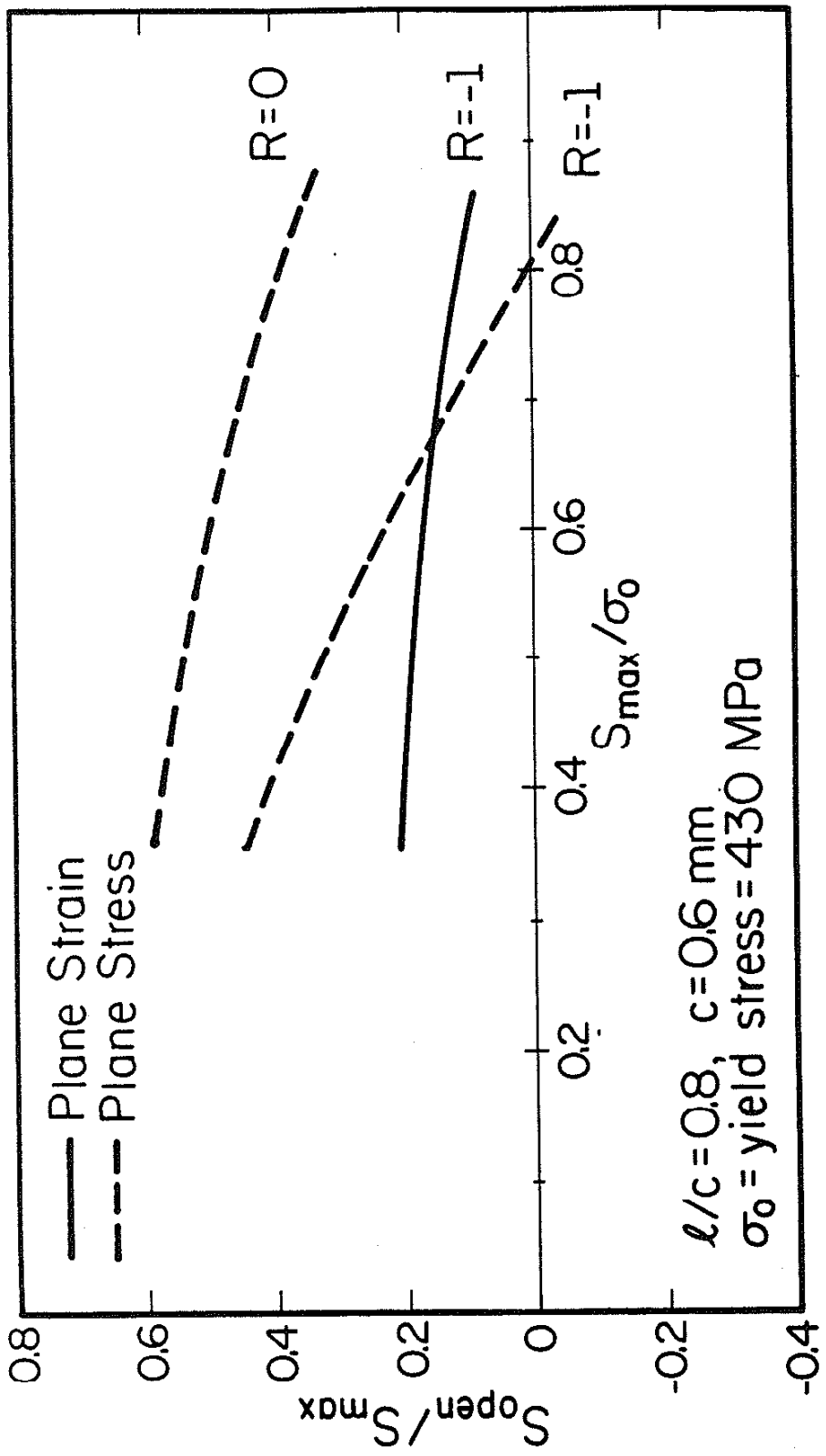

Figure 16 Normalized Crack Opening Stress as a Function of Applied Stress

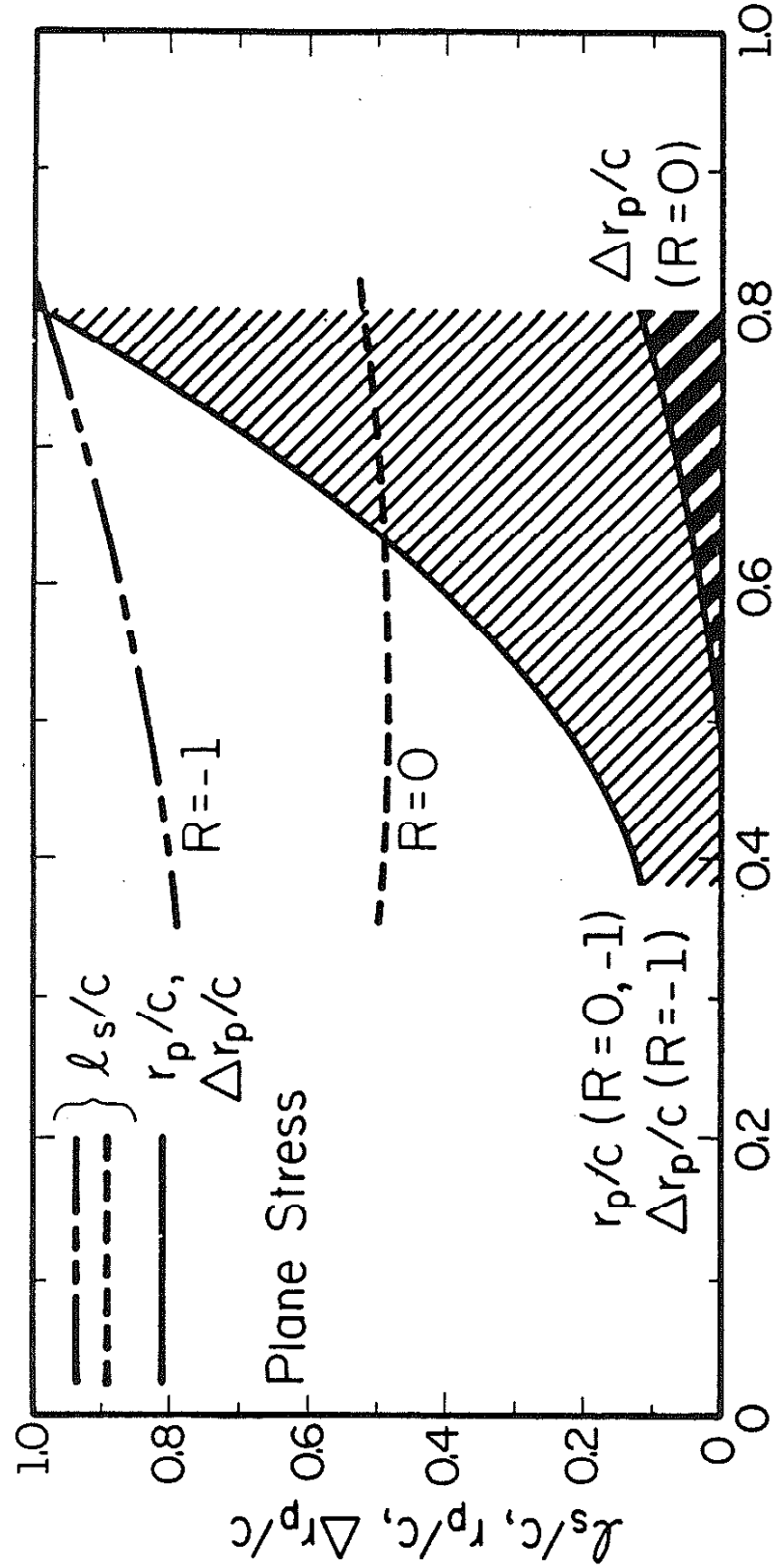

Figure 17 Stabilized Crack Length, and Maximum and Reversed Notch Plastic Zone as a Function of Applied Stress (Plane Stress)

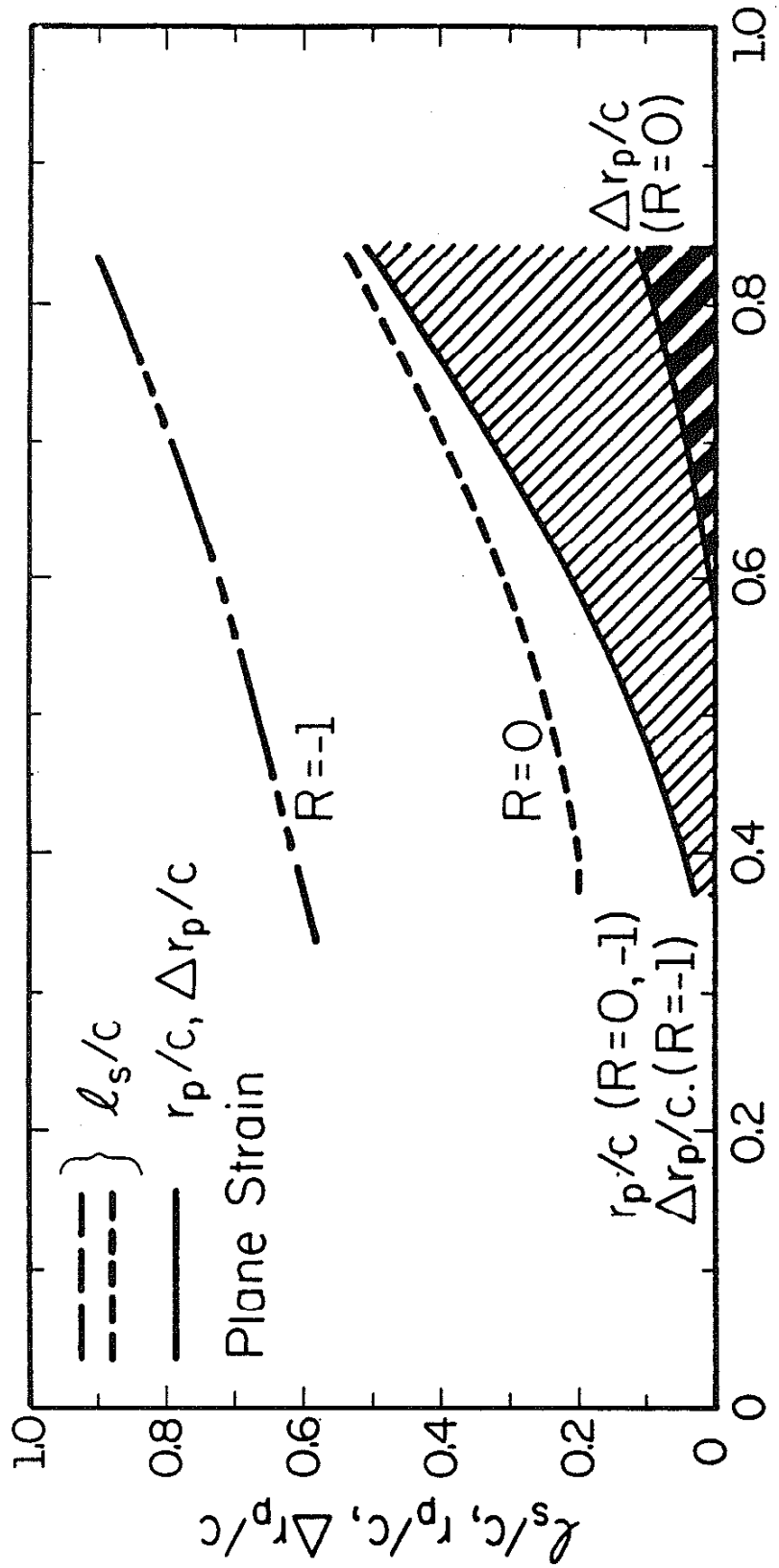

Figure 18 Stabilized Crack Length, and Maximum and Reversed Notch Plastic Zone as a Function of Applied Stress (Plane Strain)

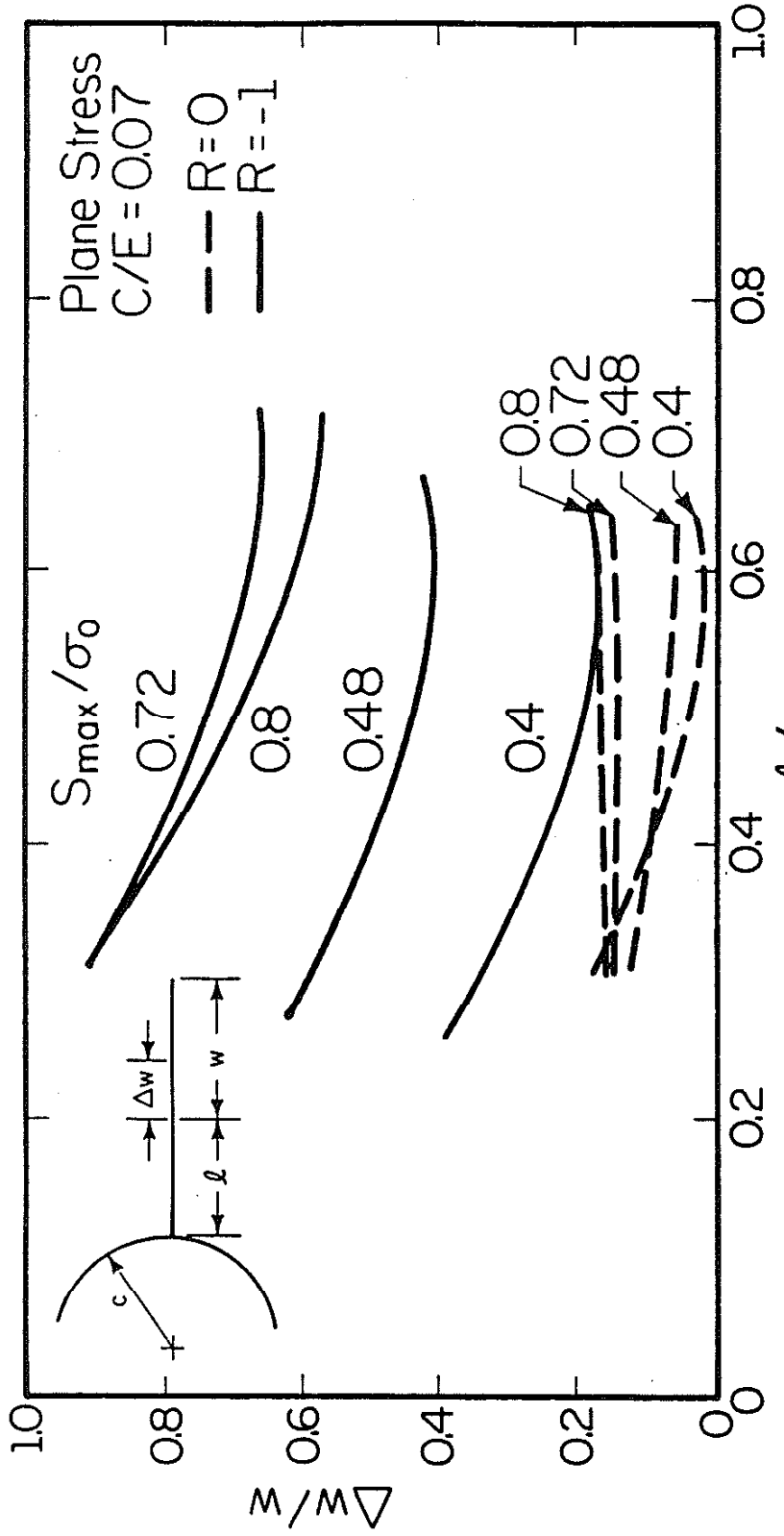

Figure 19 Ratio of Reversed to Maximum Crack Tip Plastic Zone Size versus Crack Length

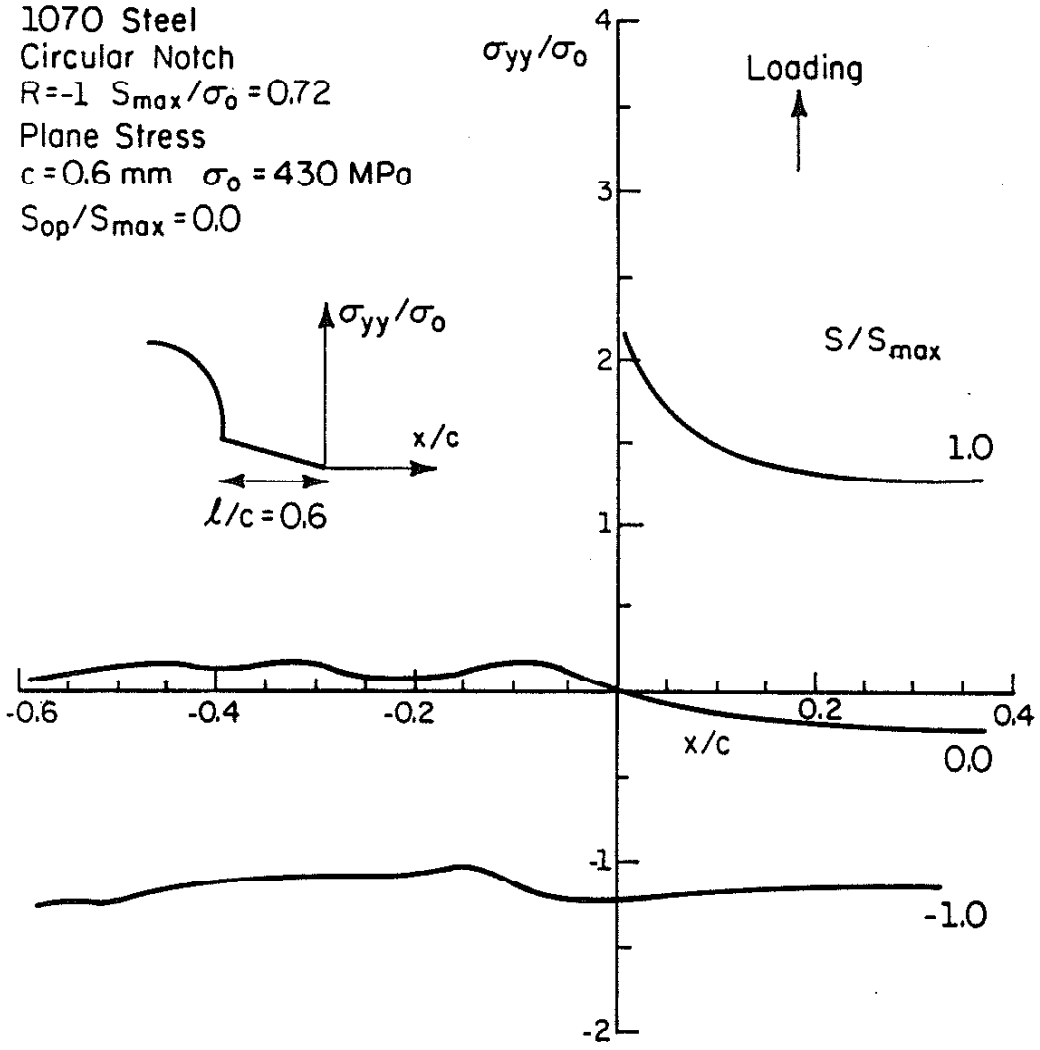

Figure 20 Near Crack Stress Fields During Different Stages of Loading (Plane Stress)

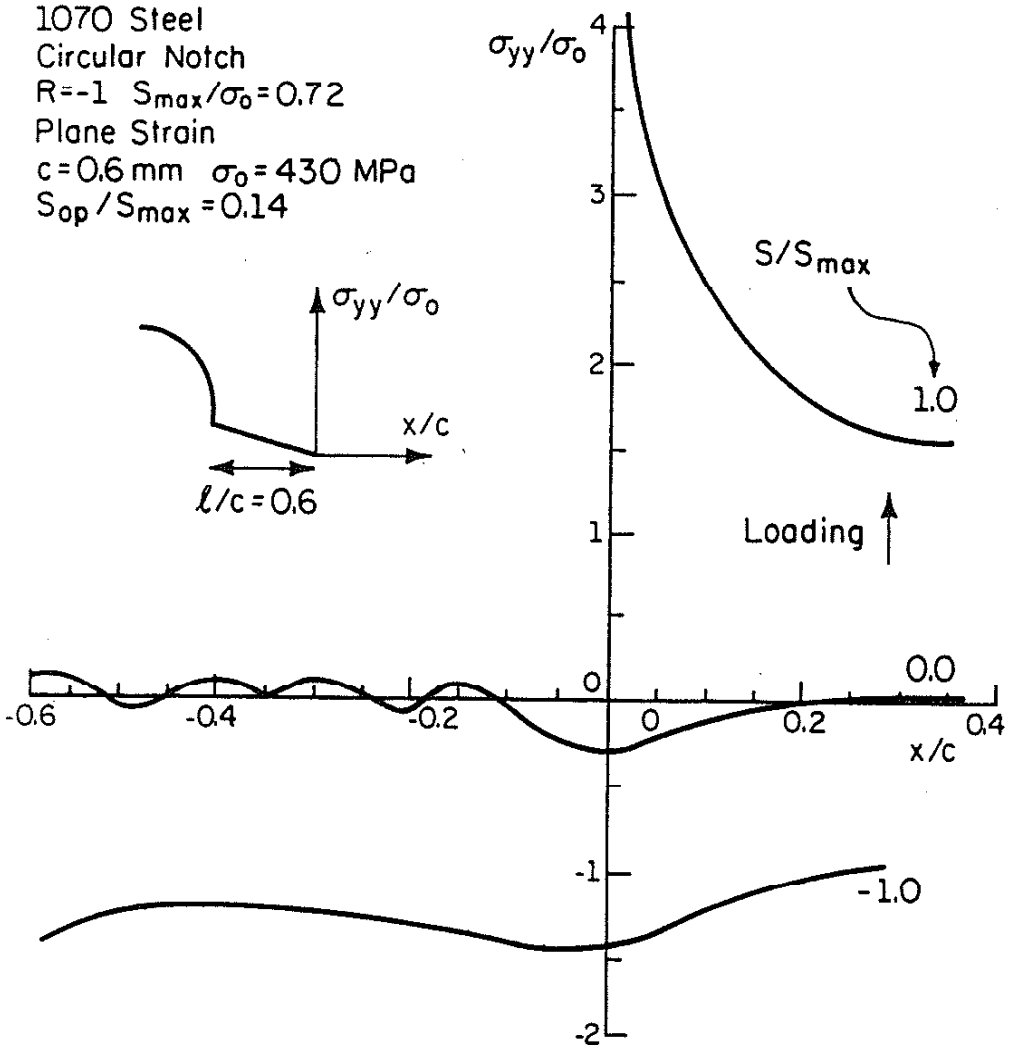

Figure 21 Near Crack Stress Fields During Different Stages of Loading (Plane Strain)

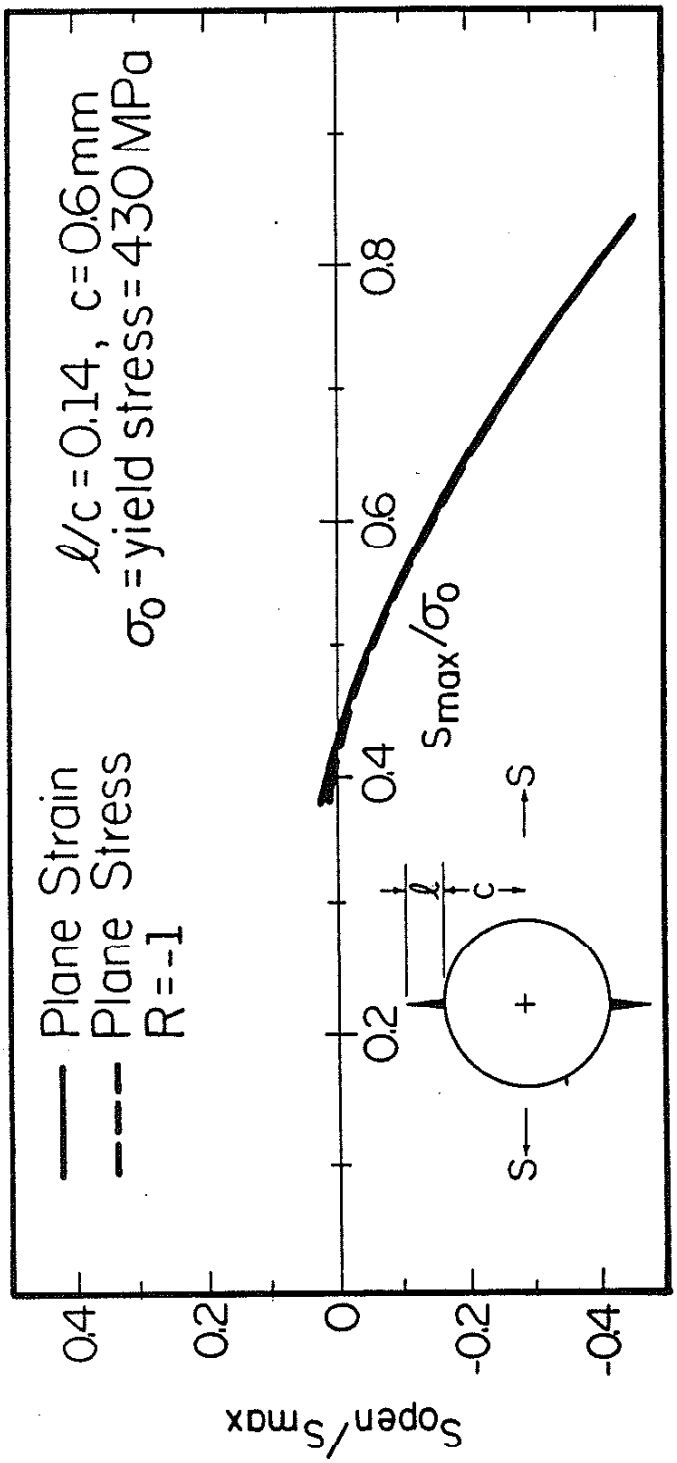

Figure 22 Normalized Crack Opening Stress as a Function of Applied Stress (ℓ/c = 0.14)

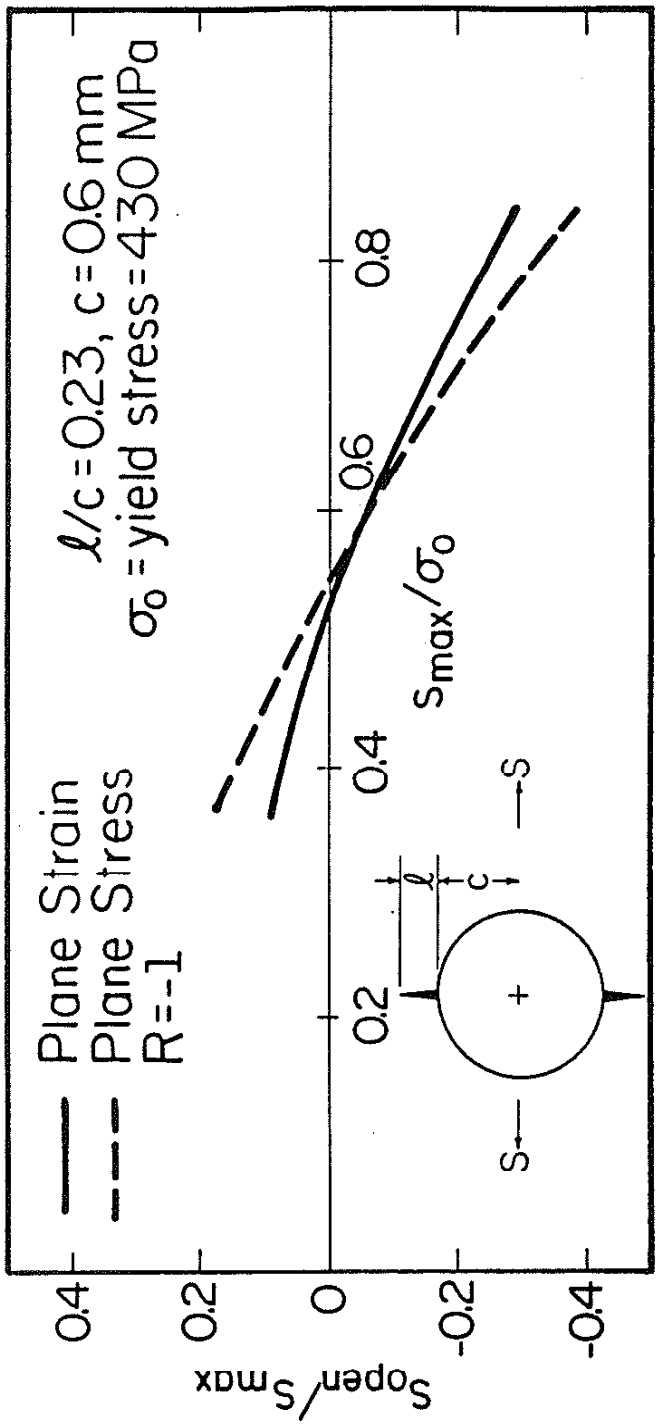

Figure 23 Normalized Crack Opening Stress as a Function of Applied Stress (ℓ/c = 0.23)

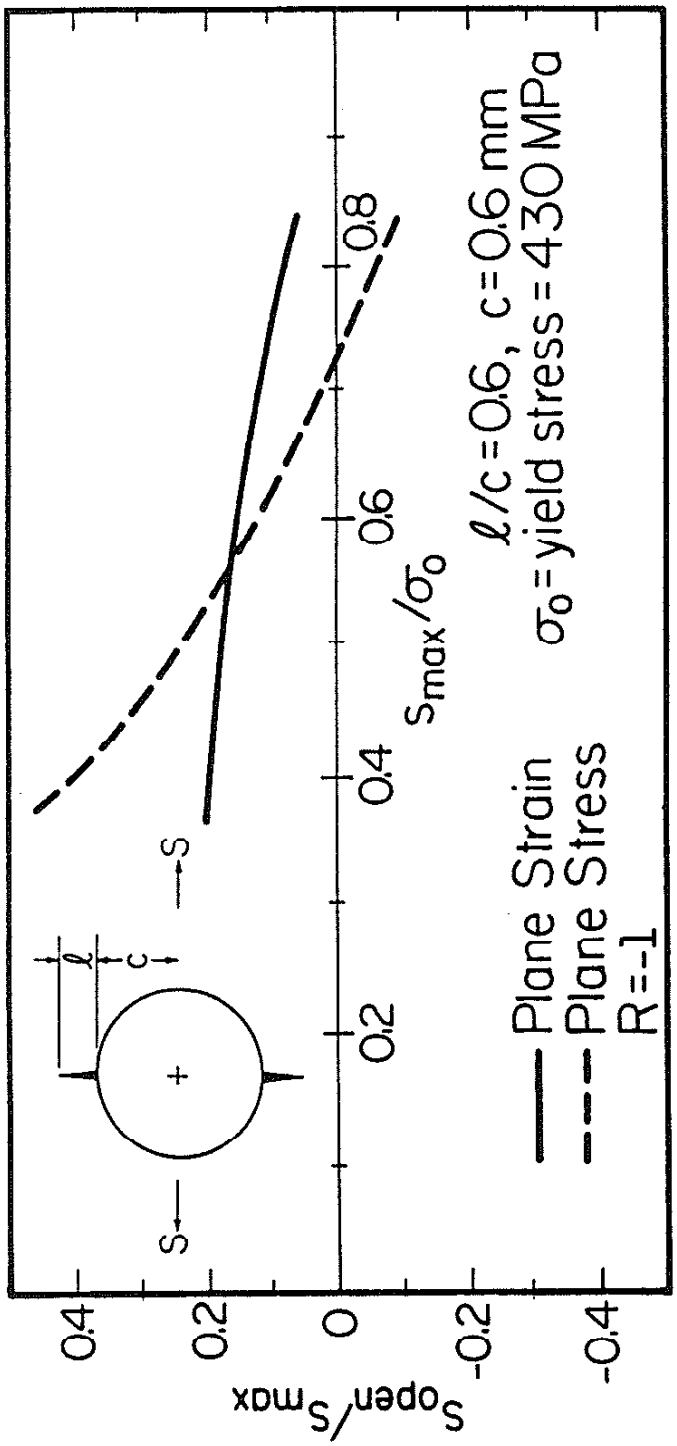

Figure 24 Normalized Crack Opening Stress as a Function of Applied Stress (ℓ/c = 0.6)

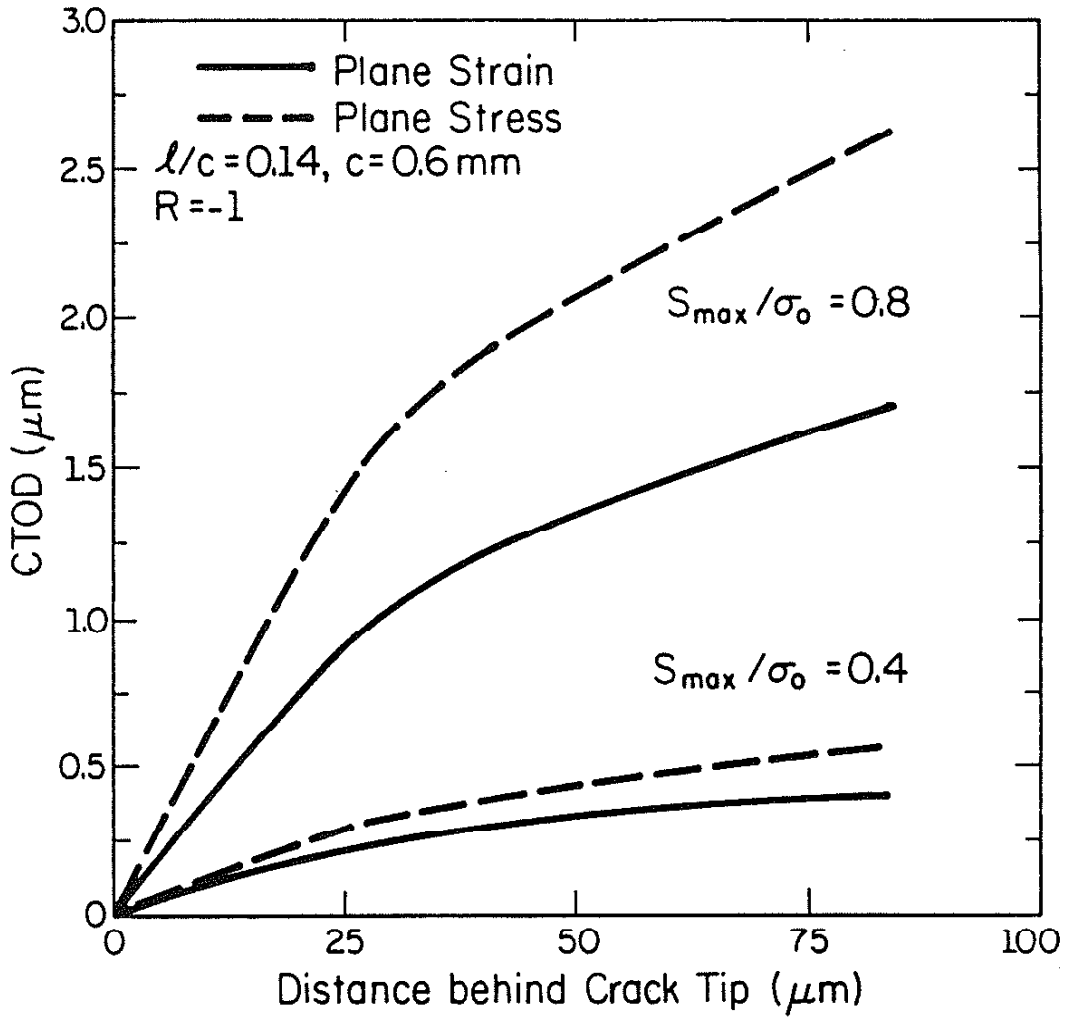

Figure 25 Crack Surface Profiles
Plane Stress versus Plane Strain (ℓ/c = 0.14)

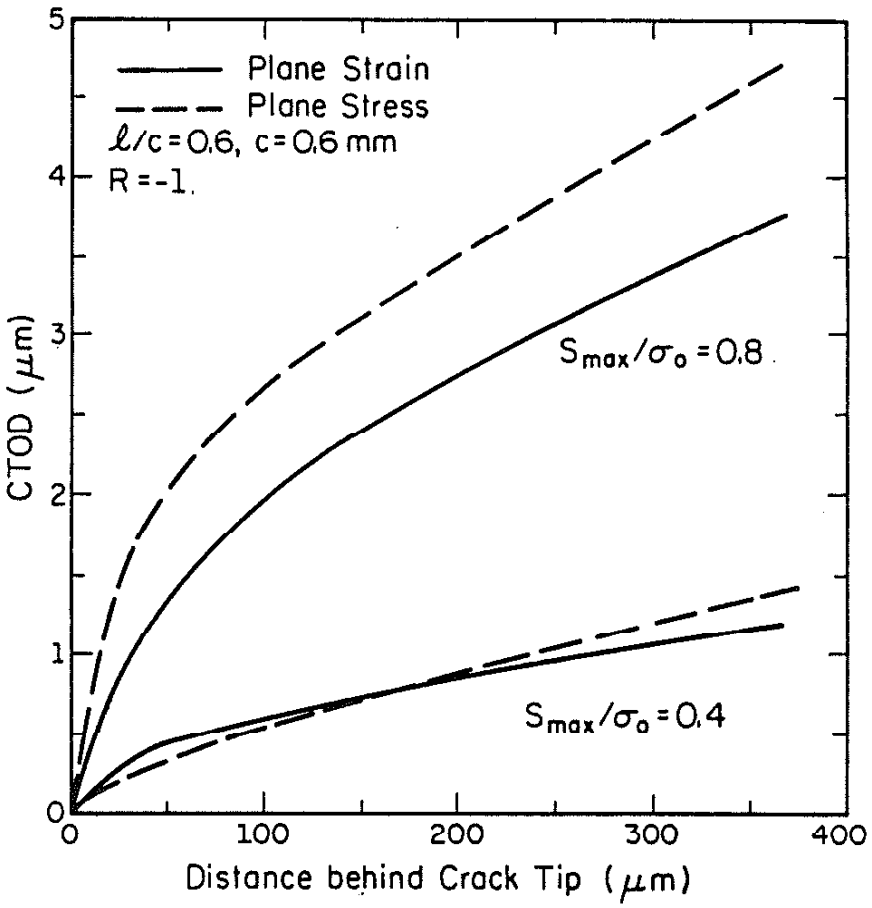

Figure 26 Crack Surface Profiles
Plane Stress versus Plane Strain (ℓ/c = 0.6)

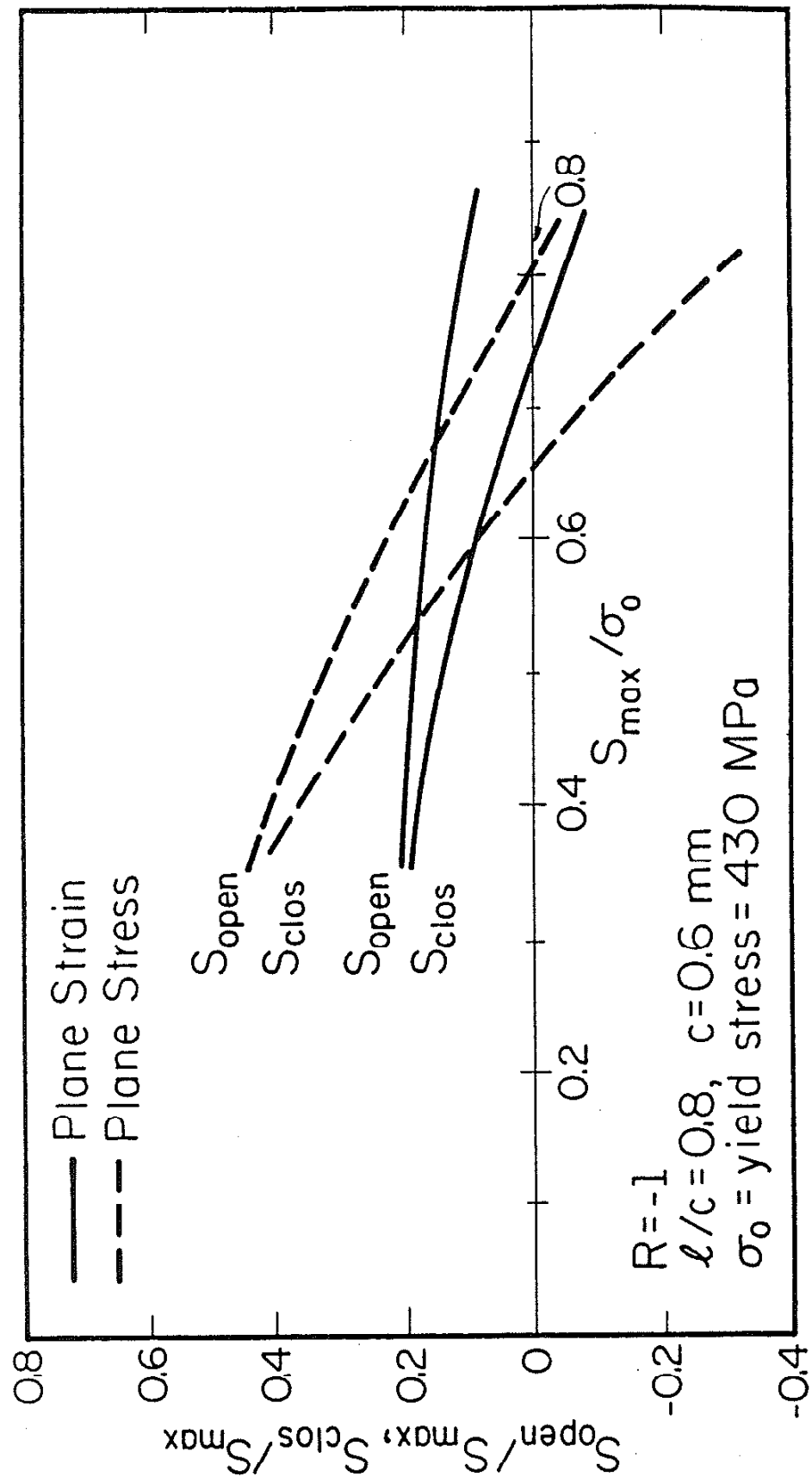

Figure 27 Normalized Crack Opening and Closure Stress as a Function of Applied Stress ($\ell/c = 0.8$)

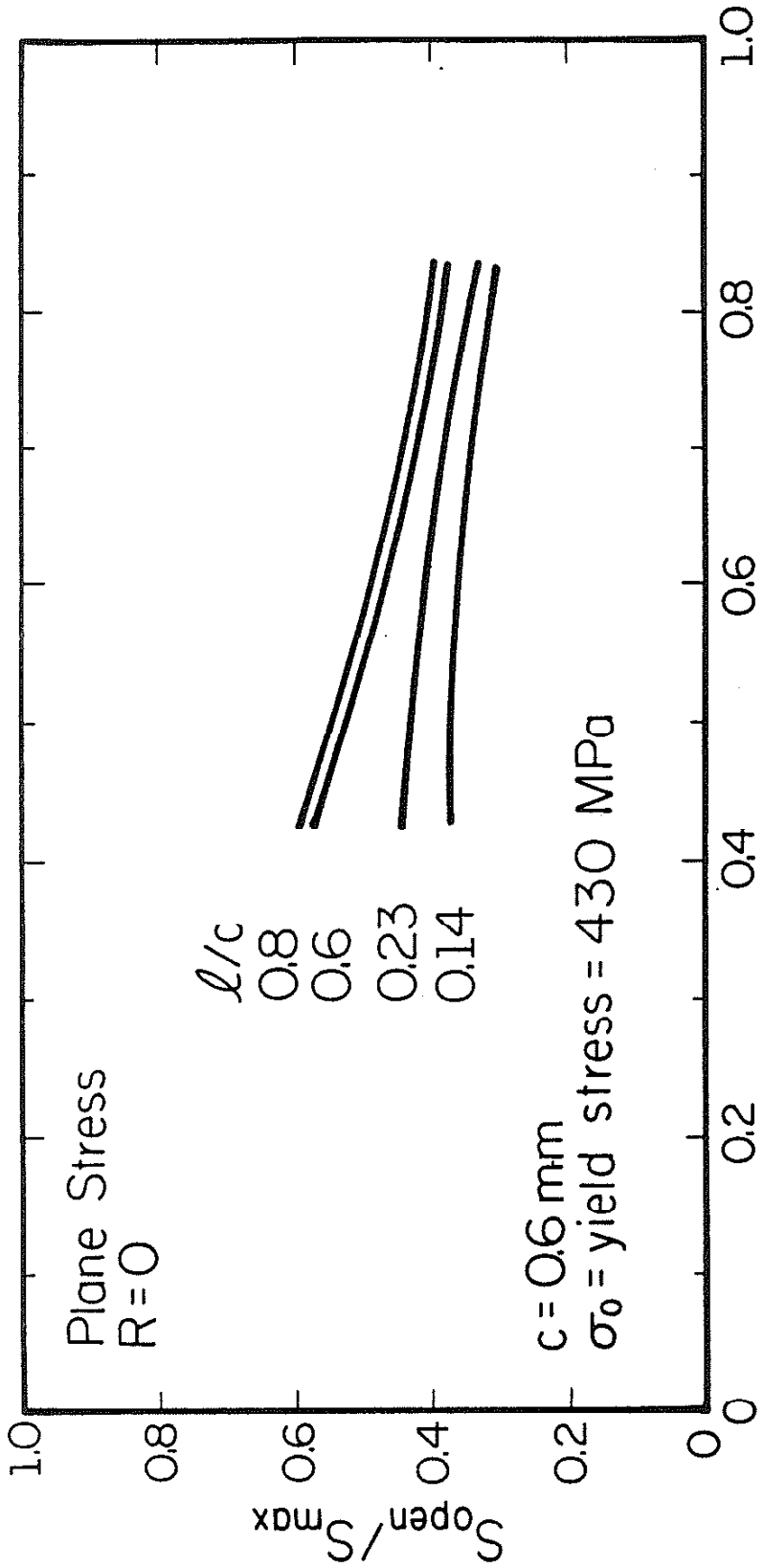

Figure 28 Normalized Crack Opening and Closure Stress as a Function of Applied Stress (R = 0)

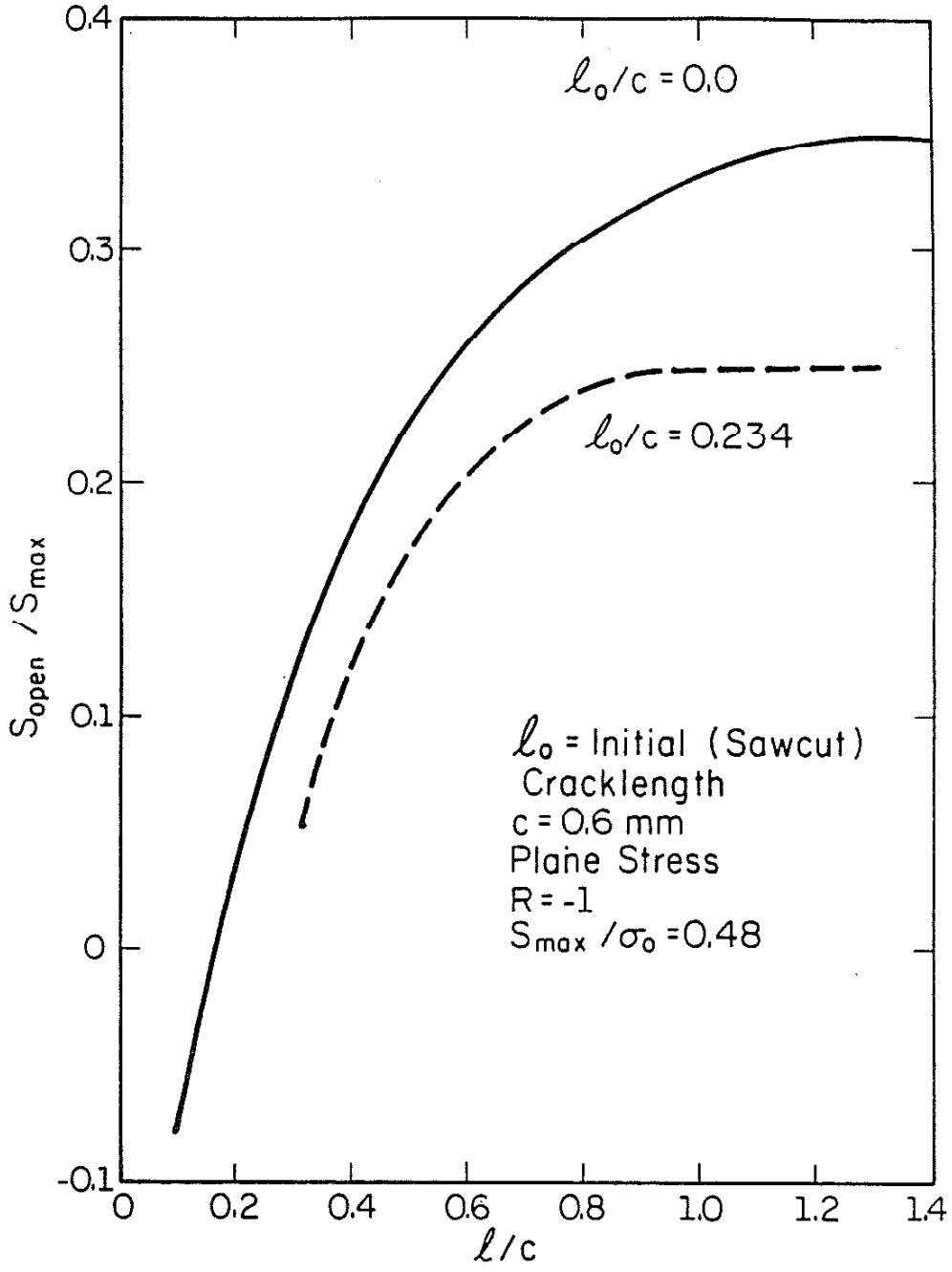

Figure 29 Numerical Crack Opening Levels as Crack Grows from Notch ($\ell_o/c = 0.0$) and from an Initial Sawcut Crack ($\ell_o/c = 0.234$)

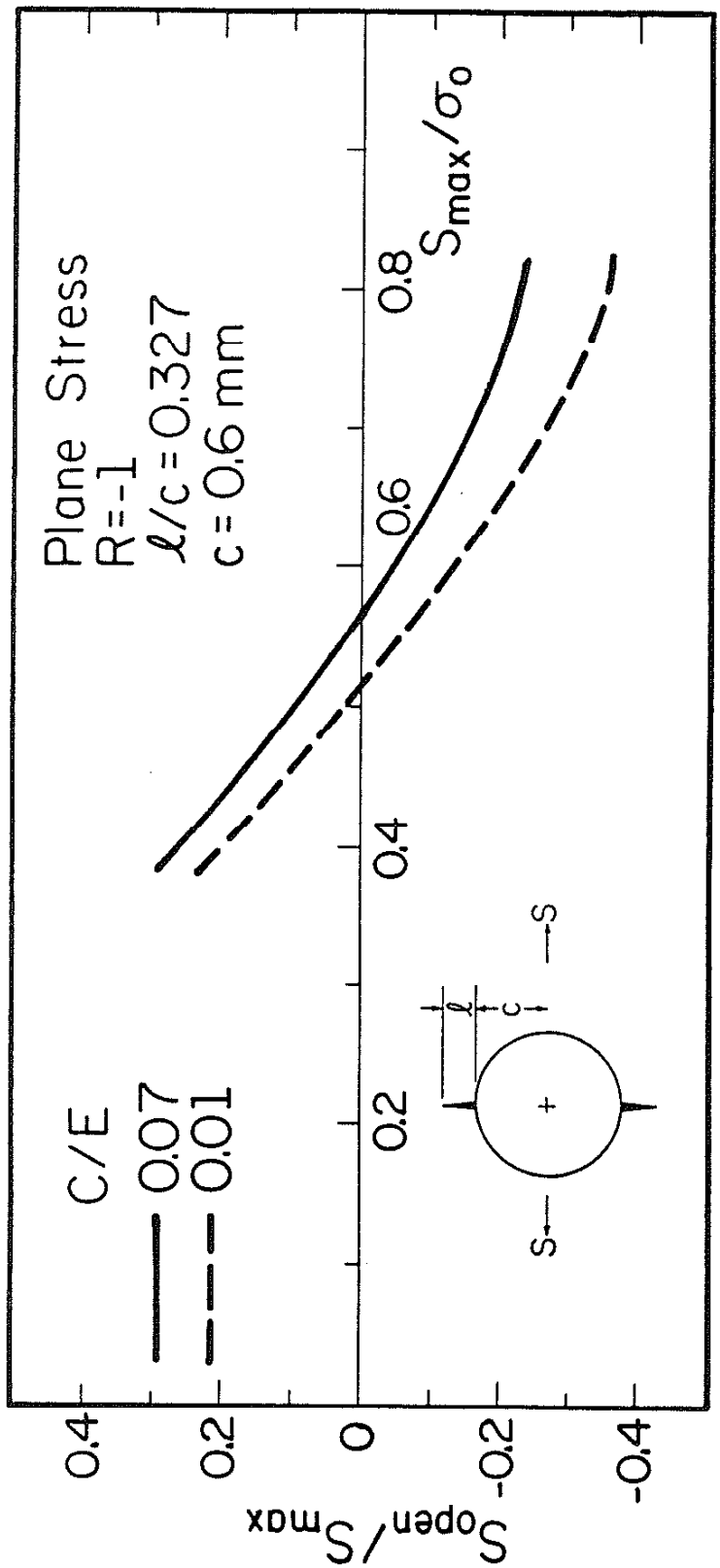

Figure 30 Normalized Crack Opening Stress as a Function of Applied Stress (Plane Stress)

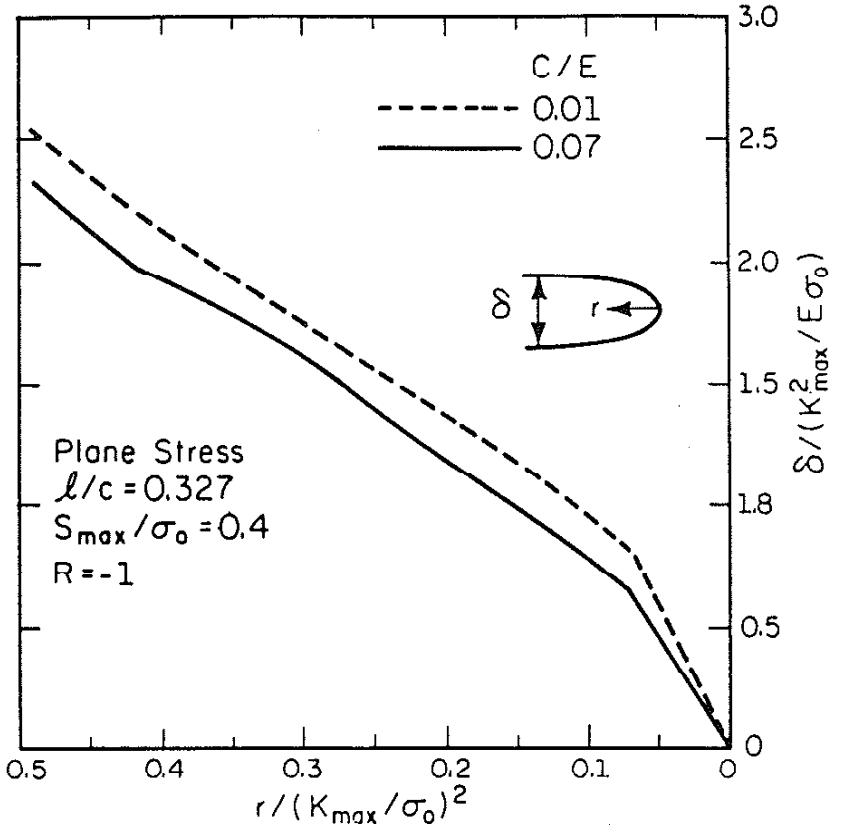

Figure 31 Crack Surface Profiles (Plane Stress)

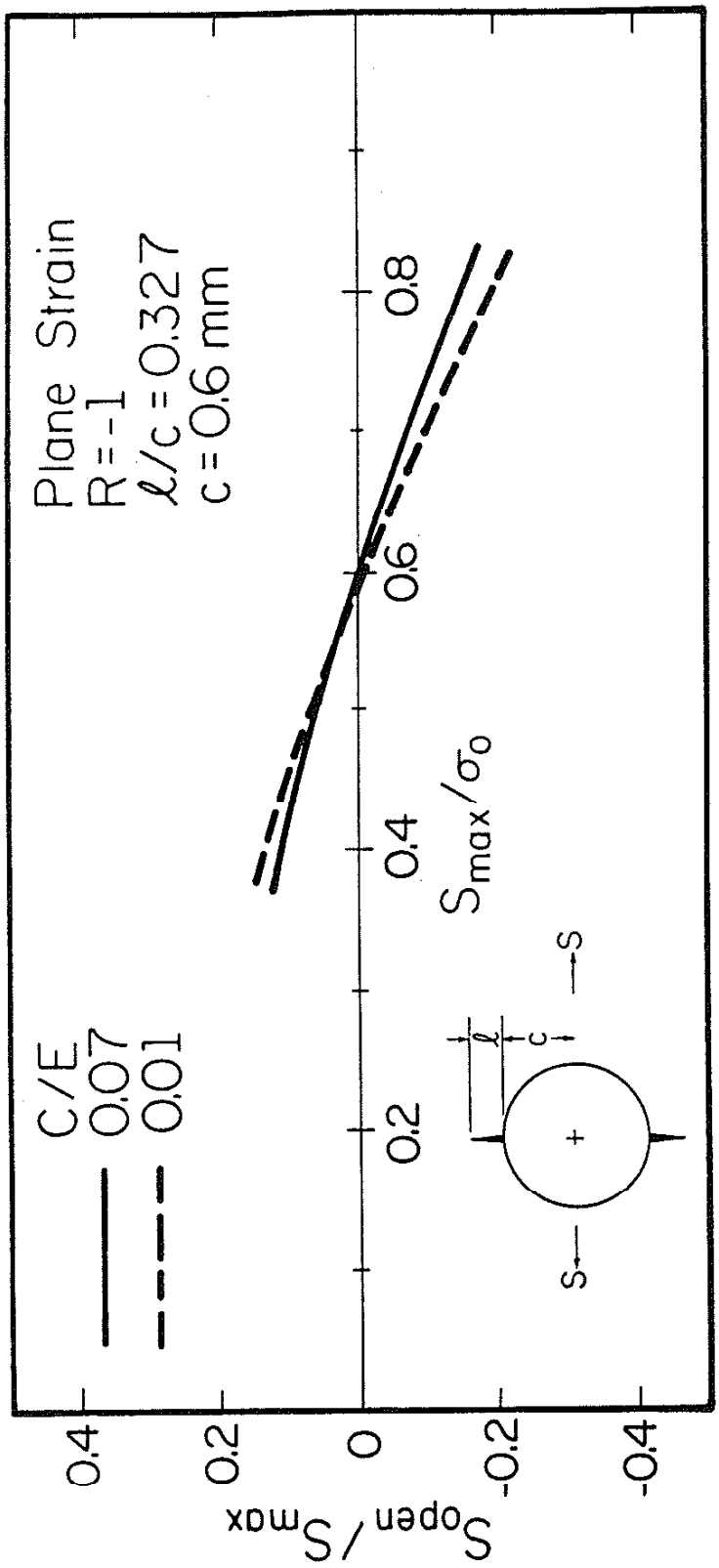

Figure 32 Normalized Crack Opening Stress as a Function of Applied Stress (Plane Strain)

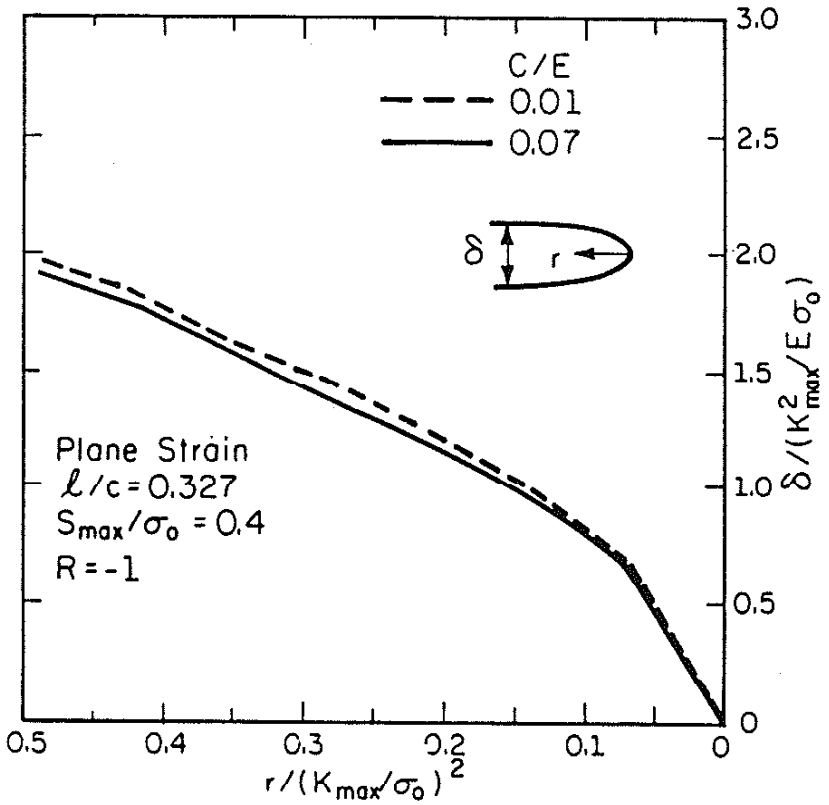

Figure 33 Crack Surface Profiles (Plane Strain)

REFERENCES

[1] Elber, W., "Fatigue Crack Propagation," Ph.D. Thesis, University of New South Wales, Australia, 1968.

[2] Elber, W., "Fatigue Crack Closure Under Cyclic Tension," Engineering Fracture Mechanics, Vol. 2, 1970, pp. 37-45.

[3] Elber, W., "The Significance of Fatigue Crack Closure." Damage Tolerance in Aircraft Structures, ASTM STP 486, American Society for Testing and Materials, Philadelphia, 1971, pp. 230-242.

[4] McClung, R. C., and Sehitoglu, H., "Closure Behavior of Small Cracks under High Strain Fatigue Histories," ASTM Int. Symp. on Fatigue Crack Closure, Charleston, South Carolina, 1-2 May, 1986 (to be published).

[5] Dowling, N. E., and Begley, J. A., "Fatigue Crack Growth During Gross Plasticity and the J-Integral," Mechanics of Crack Growth, ASTM STP 590, American Society for Testing and Materials, Philadelphia, 1976, pp. 82-103.

[6] Dowling, N. E., "Geometry Effects and the J-Integral Approach to Elastic-Plastic Fatigue Crack Growth," Cracks and Fracture, ASTM STP 601, American Society for Testing and Materials, Philadelphia, 1976, pp. 19-32.

[7] Mowbray, D. F., in Elastic-Plastic Fracture, ASTM STP 668, American Society for Testing and Materials, Philadelphia, 1979, pp. 736-752.

[8] Suresh, S., Zamiski, G. F., and Ritchie, R. O., "Oxide-induced Crack Closure: An Explanation for Near Threshold Corrosion Fatigue Crack Growth Behavior," Met. Trans. A 12A, pp. 1435-1443, 1981.

[9] Stewart, A. T., "The Influence of Environment and Stress Ratio on Fatigue Crack Growth at Near-Threshold Stress Intensities in Low-alloy Steels," Engng. Fracture Mech., Vol. 13, pp. 463-478, 1980.

[10] Walker, N., and Beevers, A., "A Fatigue Crack Closure Mechanism in Titanium," Fatigue Engng. Mat. Struct., Vol. 1, pp. 135-148, 1979.

[11] Minakawa, K. and McEvily, A. J., "On Crack Closure in the Near-threshold Region," Scripta Met., Vol. 15, pp. 633-636, 1981.

[12] Ritchie, R. O., and Suresh, S., "Some Considerations on Fatigue Crack Closure at Near-threshold Stress Intensities Due to Fracture Surface Morphology," Met. Trans., A 13A, pp. 937-940, 1982.

[13] Lindley, T. C. and Richards, C. E., "The Relevance of Crack Closure to Fatigue Crack Propagation," Materials Science and Engineering, Vol. 14, 1974, pp. 281-293.

[14] Ewalds, H. L. and Furnee, R. T., "Crack Closure Measurement Along the Fatigue Crack Front of Center Cracked Specimens," International Journal of Fracture, Vol. 14, 1978, p. R53.

[15] Fleck, N. A., and Smith, R. A., "Crack Closure-Is it Just a Surface Phenomenon," Int. J. Fatigue, Vol. 4, No. 3, pp. 157-160, 1982.

[16] Newman, J. C. Jr., "A Crack-Closure Model for Predicting Fatigue Crack Growth Under Random Loading," Methods and Models for Predicting Crack Growth Under Random Loading, ASTM STP 748, American Society for Testing and Materials, Philadelphia, 1981, pp. 53-84.

[17] Macha, D. E., Corbly, D. M., and Jones, J. W., "On the Variation of Fatigue-crack-opening Load with Measurement Location," Experimental Mechanics, Vol. 19, 1979, pp. 207-213.

[18] Dugdale, D. S., "Yielding of Steel Sheets Containing Slits," Journal of the Mechanics and Physics of Solids, Vol. 8, 1960, pp. 100-104.

[19] Sehitoglu, H., "Characterization of Crack Closure," ASTM 16th Symposium on Fracture Mechanics, ASTM STP 868, Columbus, Ohio, 1983, pp. 361-380.

[20] Sehitoglu, H., "Crack Opening and Closure in Fatigue," Engineering Fracture Mechanics, Vol. 21, No. 2, 1985, pp. 329-339.

[21] Budiansky, B., and Hutchinson, J. W., "Analysis of Closure in Fatigue Crack Growth," Journal of Applied Mechanics, Vol. 45, 1978, pp. 267-276.

[22] Dill, H. D. and Saff, C. R., "Spectrum Crack Growth Prediction Method Based on Crack Surface Displacement and Contact Analysis," Fatigue Crack Growth under Spectrum Loads, ASTM STP 595, American Society for Testing and Materials, Philadelphia, 1976, pp. 306-319.

[23] Newman, J. C. Jr., "A Nonlinear Fracture Mechanics Approach to the Growth of Small Cracks," presented at the AGARD Specialist Meeting on Behavior of Short Cracks in Airframe Components, Toronto, Canada, 1982.

[24] Fuhring, H. and Seeger, T., "Dugdale Crack Closure Analysis of Fatigue Cracks Under Constant Amplitude Loading," Eng. Fracture Mechanics, Vol. 11, pp. 99-122, 1979.

[25] Hoffman, M. and Seeger, T., "Dugdale Solutions for Strain Hardening Materials," presented at the Workshop on the CTOD-Methodology, GKSS Research Center, Geesthacht, F. R. G, 1985.

[26] Theocaris, P.S., and Gdoutos, E.E., "The Modified Dugdale-Barenblatt Model Adapted to Various Fracture Configurations in Metals," Int. Journ. of Fracture, Vol. 10, 1974, pp. 549-564.

[27] Newman, J. C. Jr., "A Finite Element Analysis of Fatigue Crack Closure," Mechanics of Crack Growth, ASTM STP 590, American Society for Testing and Materials, Philadelphia, 1976, pp. 281-301.

[28] Socie, D. F., "Prediction of Fatigue Crack Growth in Notched Members under Variable Amplitude Loading Histories," Engineering Fracture Mechanics, Vol. 9, No. 4, pp. 849-865, 1977.

[29] Ohji, K., Ogura, K., and Ohkuba, Y., "Cyclic Analysis of a Propagating Crack and its Correlation with Fatigue Crack Growth," Engineering Fracture Mechanics, Vol. 17, 1975, pp. 457-464.

[30] Lalor, P., Sehitoglu, H., and McClung, R. C., "Mechanics Aspects of Small Crack Growth from Notches--The Role of Crack Closure," presented at Second Symp. on Short Fatigue Cracks, Sheffield, U.K., Sept. 1985 (to be published).

[31] Blom, A.F. and Holm, D.K., "An Experimental and Numerical Study of Crack Closure," Engineering Fracture Mechanics, Vol. 22, 1985, pp. 997-1011.

[32] Zienkiewicz, O. Z., The Finite Element Method, 3rd Edition, McGraw-Hill, London, 1977.

[33] Ziegler, H., "A Modification of Prager's Hardening Rule," Quarterly of Applied Mathematics, Vol. XVII, No. 1, pp. 55-65, 1959.

[34] ABAQUS, Theory Manual, Version 4, 1982, Hibbit, Karlson, and Sorenson Inc., Providence, RI 02906.

[35] Timoshenko S. P., and Goodier, J. N., Theory of Elasticity, McGraw-Hill Book Company, New York, 1934.

[36] Rice, J. R., and Tracey, D. M., "Computational Fracture Mechanics," Numerical and Computer Methods in Structural Mechanics, (edited by S. J. Fenves, N. Perrone, A.R. Robinson, and W. C. Schnobrich), pp. 585-623, Academic Press, New York, 1973.

[37] Krieg, R. D., and Krieg, D. B., "Accuracies of Numerical Solution Methods for the Elastic-Perfectly Plastic Model," Journal of Pressure Vessel Technology, ASME, 99, 1977, pp. 510-515.

[38] Schreyer, H. L., Kulak, R. L., and Kramer, J. M., "Accurate Numerical Solutions for Elastic-Plastic Models," Journal of Pressure Vessel Technology, ASME, 101, 1979, pp. 226-234.

[39] Nayak, G. C., and Zienkiewicz, O. C., "Elasto-Plastic Stress Analysis. A Generalization for Various Constitutive Relations Including Strain Softening," International Journal for Numerical Methods in Engineering, Vol. 5, 1972, pp. 113-135.

[40] Sehitoglu, H., "Fatigue Life Prediction of Notched Members Based on Local Strain and Elastic Plastic Fracture Mechanics Concepts," Engineering Fracture Mechanics, Vol. 18, No. 3, 1983, pp. 609-621.

[41] Dowling, N. E., "Notched Member Fatigue Life Predictions Combining Crack Initiation and Propagation," Fatigue Engng. Mat. Struct., Vol. 2, pp. 129-138, 1979.

[42] McClung, R. C., "Behavior of Short Cracks Under Low Cycle Block Loading Fatigue Histories," M.S. Thesis, Dept. of Theoretical and Applied Mechanics, University. of Illinois at Urbana, Illinois, 1984.

[43] Kurihara, M., Katoh, A. and Kawahara, M., "Analysis on Fatigue Crack Growth Rates Under a Wide Range of Stress Ratios," Journal of Pressure Vessel Technology, Vol. 108, 1986, pp. 209-213.

[44] Leis, B.N., "Displacement Controlled Fatigue Crack Growth in Inelastic Notch Fields: Implications for Short Cracks," Engng. Fracture Mech., Vol. 22, pp. 279-293, 1985.

[45] Hammouda, M. M., Smith, R. A., and Miller, K.J., "Elastic-Plastic Fracture Mechanics for Initiation and Propogation of Notch Fatigue Cracks," Fatigue of Engineering Materials and Structures, Vol. 2, 1979, pp. 139-154.